7-17-2015 12:00 AM

Synthesis and Evaluation of a Novel Polymer Microfiber Drug Delivery System

Julie La
The University of Western Ontario

Supervisor
Dr. Wankei Wan
The University of Western Ontario

Graduate Program in Biomedical Engineering
A thesis submitted in partial fulfillment of the requirements for the degree in Master of Engineering Science

SYNTHESIS AND EVALUATION OF A NOVEL POLYMER MICROFIBER DRUG DELIVERY SYSTEM

(Thesis format: Monograph)

by

Julie La

Graduate Program
in
Biomedical Engineering

A thesis submitted in partial fulfillment
of the requirements for the degree of
Master of Engineering Science

The School of Graduate and Postdoctoral Studies
The University of Western Ontario
London, Ontario, Canada

ABSTRACT

Skin cancer is the most prevalent cancer diagnosis worldwide. Squamous cell carcinoma (SCC) is one of the most common diagnoses. Fortunately, these cancers are rarely fatal if detected and treated early on. However, current treatment options can be painful, disfiguring and can require long-term treatment courses, resulting in poor patient compliance and cancer progression. Since SCC begins as precancerous lesions, an opportunity exists for early preventative interventions which this work aims to address. We produced stabilized microfibers via centrifugal spinning and UV photocrosslinking composed of poly(ethylene oxide) functionalized with cinnamoyl chloride. Curcumin, a molecule known for its anti-cancer properties was loaded into the stabilized fibers and exhibited sustained release. The dose-dependent effect of free curcumin on A549 cancer cells was investigated. This work demonstrates the potential for this system as a transdermal delivery device for the treatment of skin cancer.

Keywords

Poly(ethylene oxide), cinnamoyl chloride, UV photocrosslinking, microfibers, centrifugal spinning, curcumin, transdermal, drug delivery, cancer

ACKNOWLEDGEMENTS

This work as a whole, and the past two years was only made possible by many important people. First off, I would like to thank my supervisor, Dr. Wankei Wan for providing me with this opportunity and confidence to learn and discover within a discipline outside of my undergraduate training. Although busy, Dr. Wan made himself as available as possible for academic and non-academic discussions to spark ideas and provide support. His ability to teach, inspire and motivate has been a major part of my experience.

In recognition of those who helped me directly with this work, I would like to thank Helium Mak for his indispensable role in supporting the development of our centrifugal spinning set-up and taking it above and beyond expectations. I would like to thank Dr. Solmaz Karamdoust for her assistance in developing the chemistry, characterization and discussions about data interpretation. I am grateful for both of your support and positive attitudes. I would like to thank Melissa Salem for her help during “crunch” time. I would also like to thank Betty Li and Helium for the design of the UV crosslinking set-up which was used for this work.

I would like to acknowledge and thank Dr. Jim Koropatnick and Dr. Saman Maleki for sharing their knowledge and putting forth the effort to train me and allow me to perform cell culture studies in a very short period of time. I would like to thank Karen Nygard for her help in training me to use the SEM in the Biotron for the preparation of images for this work.

I would like to thank my advisory committee members Dr. John de Bruyn and Dr. Lauren Flynn for their guidance and suggestions. And Dr. de Bruyn for his assistance with the fluorescence microscope.

I would like to acknowledge all the members of the Wan Lab and my peers in the BME program for their positive contributions to this experience. The conversations, times at the Grad Club and other events are memories that I will carry with me as I move forward. Specifically, I would like to thank Dawn Bannerman, Betty Li, Adrianna Mika and Asha Parekh for their friendship and support throughout this time and will be forever grateful for these relationships.

I would like to recognize my immediate and extended family for their unwavering support of my endeavours. Specifically, I would like to thank my sisters Joanne and Jennie, my parents Mai and Nam La for their love and support despite my being away from home for so long. The weekend trips home were key to my happiness and re-energized me before taking on another period of work and school. Finally, I would like to thank my boyfriend and partner in all aspects, Matt Piaseczny for his constant love and support of my ambitions. It has been quite the journey so far and I am so unbelievably grateful for his help and companionship.

TABLE OF CONTENTS

LIST OF TABLES

LIST OF FIGURES

LIST OF APPENDICES

LIST OF ABBREVIATIONS

Name	Abbreviation
actinic keratosis	AK
minimum essential medium alpha medium	AMEM
activating protein 1	AP-1
cinnamoyl chloride	CC
cyclooxygenase 2	COX-2
drug delivery system	DDS
deoxyribonucleic acid	DNA
differential scanning calorimetry	DSC
1,1'-diphenyl-2-picrylhydrazyl	DPPH
epidermal growth factor receptor 1	EGFR1
fetal bovine serum	FBS
federal drug administration	FDA
fibroblast growth factor	FGF
Fourier transform infrared spectroscopy	FTIR
glutathione s-transferase	GSTα
water	H_2O
inhibitory concentration	IC
matrix metallproteinase	MMP
messenger ribonucleic acid	mRNA
nuclear factor kappa B	NF-κB
nuclear magnetic resonance	NMR
non-melanoma skin cancer	NMSC
poly(ethylene glycol)	PEG
poly(ethylene oxide)	PEO
Peroxisome proliferator activated receptor gamma	PPAR-ɣ

scanning electron microscopy	SEM
squamous cell carcinoma	SSC
12-*O*-tetradecanoylphorbol-13-acetate	TPA
ultraviolet	UV
vascular endothelial growth factor	VEGF

1. INTRODUCTION

1.1. Motivation

Skin cancer is the most prevalent cancer diagnosis worldwide [1, 2], affecting approximately 2-3 million people annually [3]. Squamous cell carcinoma (SCC), a non-melanoma skin cancer is one of the most common diagnoses. Fortunately, these cancers are rarely fatal if detected and treated early during its progression. However, current treatment options available such as surgery, cryotherapy and topical creams can often be painful, disfiguring, require long-term treatment courses and can cause local skin reactions. Due to these factors, patient compliance suffers [4], resulting in unnecessary cancer progression. Therefore, there exists a need for an effective novel treatment option which permits patient compliance and is effective in preventing progression of precancerous lesions into an invasive, malignant state.

Overall, this thesis aims to study the chemical, physical and biological properties of photostabilized poly(ethylene oxide)(PEO)-cinnamate fibers as a carrier for curcumin to decrease cancer cell survival and proliferation.

2. LITERATURE REVIEW

2.1. Skin, Skin Cancer and Treatment Options

2.1.1. Skin

The skin is the largest organ of the body, covering approximately 1.5 - 2 m^2 and comprises 15 - 20% of the total body weight. There are three main layers of the skin, epidermis, dermis and hypodermis **(Figure 2.1)**. The epidermis is the most superficial layer, comprised of keratinocytes, stratified squamous keratinized epithelium and pigment producing melanocytes. The middle layer is the dermis, consisting mostly of connective tissue and the deepest layer is the subcutaneous layer, also known as the hypodermis. Skin can be classified as either thick or thin depending on the thickness of the epidermal layer, each with distinct functions. Thick skin is present on the palms of the hands and the soles of feet, where exposure to friction is the highest. The rest of the body covering is thin skin. The epidermis of thin skin is further divided into 4 layers, starting with the most superficial: stratrum corneum, granular layer, spinous layer and basal layer. Each layer is composed of histologically distinctive cell types which are used to identify the source pathological conditions. The skin possesses five main essential roles: protection, metabolism, sensory, thermoregulation and sexual signalling [5]. Although the skin acts as a protective barrier to UV radiation [6], excessive exposure, genetic predispositions [7] or a combination, play an additive role in the pathogenesis of skin cancers [8].

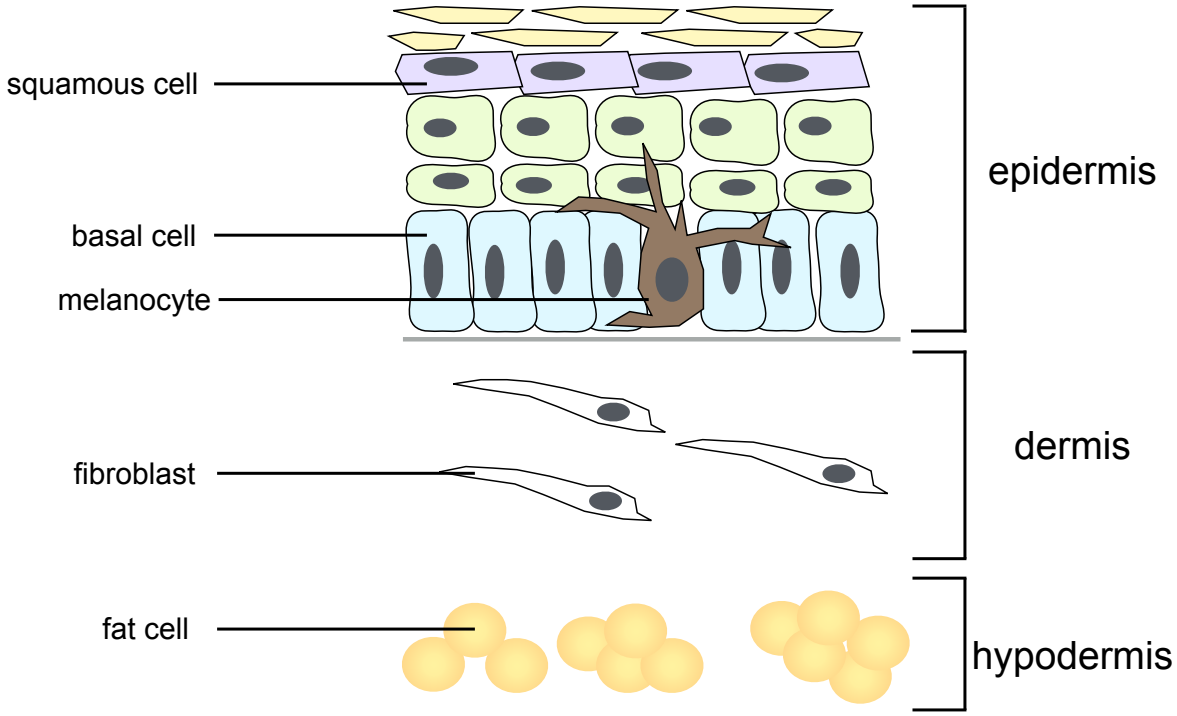

Figure 2.1: Structure of the skin, including layers and main cell types.

2.1.2. Skin Cancer

Skin cancers are defined as cancers originating from skin and are classified by the cells from which they are derived, these can be categorized into two major groups: melanoma and non-melanoma skin cancers (NMSCs). The most common subtypes of NMSCs are basal cell (BCC) and squamous cell carcinoma (SCC) [1]. Melanomas are cancers that originate from melanocytes, whereas BCC and SCC are cancers originating from basal cells and squamous cells, respectively. SCC typically begins as sun induced skin lesions called actinic keratosis (AK) [9]. A classic model for cancer pathogenesis may be used to describe the progression of actinic keratoses into SCC [10]. First, a mutation in a gene such a tumour suppressor may result in the development of this precursor lesion. Additively, mutations in proto-oncogenes may result in increased proliferative capacity leading to neoplastic properties and the

development of invasive SCC [10]. The induction of these mutations for SCC is typically from UV exposure, causing thymidine dimer [11] formation in DNA resulting in mutations [9, 12].

Epidemiologically, skin cancers and more specifically NMSCs are the most common cancer diagnoses with incidence rising worldwide. Although mention of its incidence is often neglected in worldwide cancer reports due to inconsistent reporting to cancer registries to obtain accurate estimates [13, 14]. Fortunately, the mortality rate associated with NMSCs is low when detected and treated early on during its progression. However, current treatment options are accompanied by low patient compliance due to visible side effects [15]. As a result of low patient compliance, AK have the potential to develop into invasive SCC, a larger economic and health burden. An international study on physical perceptions about current treatment options for AK revealed a need for research to address the limitations of current therapies in order to improve outcomes [15].

2.1.3. Current Treatment Options and Side Effects

In order to reduce rates of SCC, AK lesions must be managed prior to its progression into invasive cancer. Several options currently exist to treat AK. However, there does not exist a therapy which meets all the needs of the consumer: good efficacy to reduce risk of SCC, low risk of adverse effects, few dosages and short treatment time. One current option is surgical removal of lesions, but can result in scarring. Other common options include topical treatments such as 5-fluorouracil and imiquimod creams, which are less invasive but require extended treatment periods, and can lead to undesirable local skin reactions (redness, scarring, etc.). Given that these treatments require compliance for up to 16 weeks, patients may be required to manage these side effects for long periods of time, decreasing the tolerability of the treatment. The downfalls of these current treatment options result in patient non-compliance and ultimately increasing patient risk for developing invasive SCC.

Therefore, the options are to develop new drugs or alternatively improve the delivery of current drugs with fewer side effects with equivalent effectiveness are required in order to prevent NMSC progression in patients with AK.

Chemoprevention, a promising area in anti-cancer research is the administration of dietary or pharmacologic agents to inhibit or reverse carcinogenesis [16, 17]. In contrast to typical chemotherapeutics, these products present with lower side effects. Chemopreventive agents may be classified based on the stage of interference during carcinogenesis. Blocking agents act early on in the progression by inhibiting the conversion of cells from a normal to neoplastic state. Alternatively, suppressing agents inhibit proliferation and growth during cancer progression [18]. Examples of identified chemopreventive agents are vitamin A [19, 20], lycopene [21], grape seed extract [22, 23], green tea extract [24, 25] and curcumin [18, 26, 27]. The focus of this work will be on curcumin as a chemopreventive.

2.1.4. Curcumin

The naturally occurring and active components of *Curcuma longa* (turmeric) called curcuminoids are isolated from the rhizome, the root of the plant, which contains the majority of curcuminoids. The turmeric root and spice derived from it have been used as food additives, medicines, textile dyeing and cosmetics for over 2000 years [28].

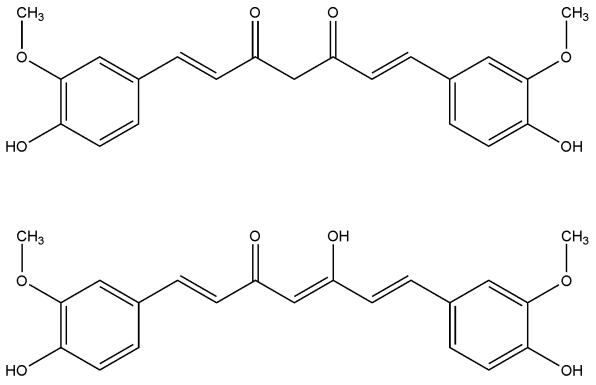

Figure 2.2: Structure of curcumin, keto (**top**) and enol (**bottom**) tautomers.

Curcumin ($C_{21}H_{20}O_6$) [1,7-bis-(4-hydroxy-3-methoxyphenyl)-1,6-heptadiene-3,5-dione] also known as diferuloylmethane and curcumin I is the principal curcuminoid and regarded as the most biologically active curcuminoid of turmeric. This molecule exists as keto-enol tautomers as a solid and in solution (**Figure 2.2**). Desmethoxycurcumin (curcumin II), bis-desmethoxycurcumin (curcumin III) and cyclocurcumin are additional chemical constituents of curcuminoids which have previously been extracted and identified [29, 30]. In general, the composition of commercial curcumin contains: ~77% of curcumin I, ~17% curcumin II and ~3% curcumin III. Curcumin I, a polyphenol providing the yellow-orange colour is a powder that is soluble in ethanol, dimethylsulfoxide and acetone but nearly insoluble in water and ether. Curcumin I possesses a molecular weight of 368.37 g/mol and a melting point of 183 °C. Commercially available turmeric and curry powders contain curcumin however, these is batch to batch variability of the purity as described by Tayyem *et al*. [31], thus it is imperative to determine the purity of curcumin to clearly establish a dose-response relationship.

Anti-Cancer and Chemopreventive Properties of Curcumin *in vitro and in vivo*

It has been demonstrated that curcumin interacts with many cellular targets including transcription factors, enzymes and growth factor receptors, ultimately resulting in altered gene expression and imparting antioxidant, anti-inflammatory and anti-cancer properties (**Table 1**). Molecules identified as chemopreventive agents are defined by their ability to arrest progression or prevent cancer development and have several commonalities including enhanced apoptosis, growth inhibition and proliferation, halting cellular invasion and inhibition of angiogenesis.

Table 1: Summary of curcumin's cellular targets [32]

General category	Target	Function of target/ Observation in cancers	Effect of curcumin
Transcription factors	Nuclear factor kappa B (NF-κB)	Suppresses apoptosis and is constitutively expressed in many cancers	Inhibits the activation of NFκB
	Activating protein-1 (AP-1)	Involved in proliferation and is constitutively expressed in many cancers	Inhibits activation of AP-1
	Peroxisome proliferator activated receptor gamma (PPAR-ɣ)	Inhibits proliferation of nonadipocytes	Activates PPAR-ɣ inhibiting cell proliferation, inducing apoptosis
	Notch-1	Maintains balance between cell proliferation, differentiation and apoptosis. Balance disrupted in cancer	Reduces levels of Notch-1
	Wnt/beta-catenin	Highly regulated signaling pathway. Often dysregulated in cancers	Inhibits pathway through reduction of nuclear β-catenin
Enzymes	Cyclooxygenase (COX-2)	Inflammatory enzyme, overexpressed in many cancers resulting in cell proliferation and inhibition of apoptosis	Inhibits expression of COX-2
	Matrix metalloproteinase (MMP)	Mediators of tumor metastasis, often upregulated in cancers	Inhibits MMP-9
Growth factors and receptors	Epidermal growth factor receptor 1 (EGFR1)	Overexpressed in cancer	Inhibits expression, act as EGFR1 antagonist
	Fibroblast growth factors (FGFs)	Overexpressed in cancer and involved in angiogenesis	Angiogenic pathway inhibited
	Vascular endothelial growth factor (VEGF)	Major role in angiogenesis and cancer growth	Inhibits expression of VEGF

Safety and pharmacological effects of oral curcumin

Curcumin is remarkably non-toxic and is well tolerated even at doses as high as 12 g/ day [33]. However, due to its hydrophobicity, water insolubility and first pass metabolism, it has poor oral bioavailability. Orally is the most common and convenient route of drug administration. In order for the drug to reach the systemic circulation it must first be absorbed by the intestinal epithelium and enter the hepatic portal system where first pass metabolism occurs. After which, drug concentrations are dramatically reduced due to metabolism in the liver and the remaining dose may finally be able to enter the systemic circulation to exert their effects [34]. Studies [33, 35] conducted to investigate oral dose-serum concentration relationships showed that curcumin and its metabolites are detectable in serum with curcumin doses greater than 4000 mg/day with a respective maximum serum concentration of 0.5±0.11 μM. This serum level peaked one to two hours following oral intake and declined within 12 hours. Doses below 4000 mg/day were undetectable in serum. The anti-cancer properties of curcumin are most pronounced in and near the gastrointestinal tract when orally administered and are most effective against cancers of such tissues. Garcea et *al.* [34] suggest that although curcumin is an effective chemopreventive agent *in vitro*, the oral dose required for concentrations with effective pharmacological activity are likely not feasible in humans. These studies provide a thorough investigation into the poor oral bioavailability of curcumin. Thus, there is a need for improved delivery to maximize the benefits for this effective chemopreventive agent.

Curcumin as an iron chelator *in vivo*

An unexpected observation made by Jiao, Y. *et al*. [36] revealed the modulation of iron metabolism of liver cells *in vitro* suggestive of curcumin's ability to chelate iron. Two main proteins were investigated, ferritin and glutathione S-transferase (GSTα). Ferritin is a protein which maintains intracellular iron levels and a decrease in ferritin levels indicates lowered intracellular iron. GSTα is a cytoprotective enzyme which is

induced in parallel with ferritin transcription and regulates ferritin levels. In this study, liver cells were cultured in the presence of curcumin and the effects on ferritin and GSTα were measured. Curcumin induced GSTα and ferritin mRNA levels but reduced detected levels of ferritin protein. To further study this phenomena, mice were fed diets supplemented with curcumin for 12 weeks. Studies revealed a statistically significant reduction in ferritin protein levels and increase in GSTα levels in mice receiving 2% curcumin as compared to controls receiving 0% curcumin in their diets. This reduction in ferritin levels suggest reduction of intracellular iron levels and thus iron chelating ability of curcumin. Jiao, Y. *et al*. [36] further studied the impact of curcumin as an iron chelator on systemic iron levels and its impact on iron deficiency conditions. In this study, mice were fed diets containing various concentrations of iron ranging from 5 - 1000 mg/kg to establish the dose-dependent parameters of systemic iron such as plasma iron, hemoglobin, hematocrit levels and others were measured. Mice from all groups showed no statistically significant differences in such parameters. Subsequently, mice were fed diets supplemented with curcumin at concentrations ranging from 0 - 2% to study the effect of curcumin on mice receiving different amounts of iron in their diets. For mice receiving curcumin with diets containing low-iron, a significant decrease in all parameters of systemic iron was observed, suggesting iron deficiency anemia was induced by curcumin. Microcytosis, a decrease in red blood cell size indicative of anemia, was found for mice receiving diets containing low-iron with microcytosis increasing proportionally with amount of curcumin intake[37].

At this point, curcumin has the potential to chelate iron and alter systemic iron metabolism as demonstrated by studies *in vitro* and *in vivo.* Thus oral administration of curcumin may be harmful in patients with diminished iron stores due to diet, anemia or other chronic diseases. Anemia is prevalent in patients with cancer [38] and thus, orally administered curcumin may be particularly harmful in large doses to those patients. Although a study comparing oral versus topical curcumin in a skin

cancer model reported equivalent efficacy, localized treatments may be preferred over oral to avoid iron chelation complications.

Topical administration of curcumin

A method of drug administration that would avoid low oral bioavailability and potential of iron chelation in vulnerable populations would be possible in cases where local delivery of curcumin could be accomplished. One such example is externally on the skin. Curcumin's activity in preventing the progression of cancer was initially demonstrated with mice. Mice were treated with 12-*O*-tetradecanoylphorbol-13-acetate (TPA), a known inducer of skin cancer, with co-treatment of a topical curcumin paste. The effects of TPA were inhibited due to curcumin's inhibitory effect on cyclooxyrgenase activities [39]. Other studies using curcumin cream pastes note that the creams were irritating in nature causing thickening of the epidermis. This issue may be augmented in humans as side effects are one of the main causes of poor patient compliance [40, 41]. Therefore, although topical administration is preferred for some applications, there does not exist a carrier without side effects.

2.2. Drug Delivery

Drugs are of significant importance in treating diseases. One category is the chemotherapeutic drugs, a class of drugs used to treat cancer. Typically the mode of administration is intravenously and less commonly, orthotopic injection into specific sites such as the spine, by mouth as a pill or liquid or topically as a cream. Side effects of chemotherapy may be severe as a result of normal cell death along with cancer cell death. Typically, chemotherapeutic drugs are non-specific and systemic introduction into the body is the main cause of side effects [42]. Thus, targeting drug activity by either exploiting key differences between cancer and healthy tissues or localizing drug delivery is of clinical importance.

The major advantage of administering drugs using a drug delivery system is the maintenance of drug concentrations within the therapeutic range **(Figure 2.3)**.

Minimizing general exposure to these compounds is ideal, however, in order to maintain effective concentrations, smaller, more frequent administrations would be required and risk increasing plasma drug levels into the toxic range. Both inconvenience and side effects result in poor patient compliance and decrease quality of life. Thus, controlled drug delivery to maintain safe, effective concentrations is highly desired.

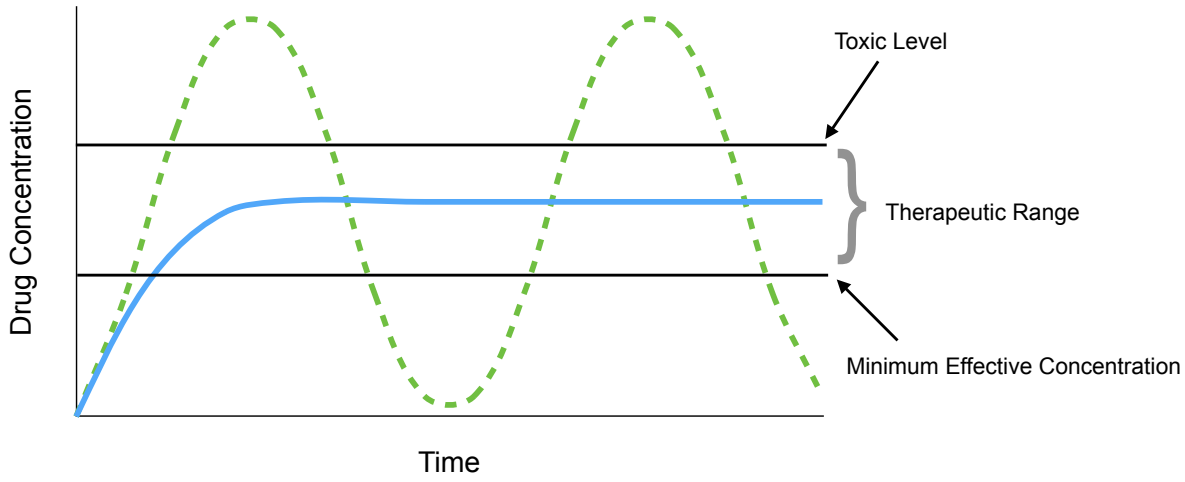

Figure 2.3: Drug concentration following drug administration with (solid line) and without (dashed line) controlled release.

Drug delivery systems (DDS) may be classified by the mechanism of release they follow: solvent activated, chemically controlled and diffusion controlled [43]. Briefly, solvent activated systems are osmotically or swelling controlled. In osmotically controlled systems, an external fluid moves against the drug concentration gradient, forcing the drug out of the device. This system works for water-soluble drugs and zero-order kinetics are possible. In swelling controlled systems, drugs are dispersed in a dry hydrophilic polymer and swell once they encounter an aqueous environment such as body fluids resulting in diffusion of drug out of the polymer. Chemically controlled delivery systems are further classified as biodegradable or pendant-chain. Biodegradable systems release the drug as the polymer disintegrates. Pendant-chain systems have drug molecules chemically bound to the polymer chains with release

dependent on cleavage of that bond. Diffusion controlled DDS can be further classified into reservoir or monolithic devices. In reservoir devices, the polymer surrounds a core of drug where release occurs by diffusion through the polymer membrane. This type of release can be described using Fick's first law (equation 1) if the membrane is non-porous. Where J is the flux/unit area, D is the diffusion coefficient through the membrane, K is the partition coefficient, ΔC is the concentration difference across the membrane and l is the thickness of the membrane.

$$J=\frac{DK\Delta C}{l} \tag{1}$$

Monolithic devices have the drug uniformly dispersed throughout an inert (non-swollen or fully swollen, and non-degrading) polymer and release is controlled by diffusion of the drug from the polymer matrix. Cumulative amount of drug released can be calculated for a thin slab using early (equation 2) and late (equation 3) time approximation equations. Where M_t is the amount of drug released at time t, M_∞ is the amount of drug loaded, D is the diffusion coefficient and l is the thickness of the slab.

$$\frac{Mt}{Mi}=4\left(\frac{Dt}{\pi l^2}\right)^{\frac{1}{2}} \quad for\ 0 \le \frac{Mt}{Mi} \le 0.6 \tag{2}$$

$$\frac{Mt}{Mi}=1-\frac{8}{\pi^2}exp\left(-\frac{\pi^2 Dt}{l^2}\right) for\ 0.4 \le \frac{Mt}{Mi} \le 1.0 \tag{3}$$

Cylindrical and spherical geometries require additional parameters in the calculations (equations 4 and 5). Release of a drug from these geometries can also be calculated using early time approximation and late time approximation. Parameters are the same as above, in addition to those, a is the radius of the cylinder or sphere. These equations were described by Baker and Lonsdale[44].

$$\frac{Mt}{Mi} = 4\left(\frac{Dt}{\pi a^2}\right)^{\frac{1}{2}} - \frac{Dt}{a^2} \quad for\ 0 \leq \frac{Mt}{Mi} < 0.4 \tag{4}$$

$$\frac{Mt}{Mi} = 6\left(\frac{Dt}{\pi a^2}\right)^{\frac{1}{2}} - \frac{3Dt}{a^2} \quad for\ 0 \leq \frac{Mt}{Mi} < 0.4 \tag{5}$$

Many applications of these drug delivery systems exist on the market today. Some examples of diffusion controlled drug delivery devices include, Progestasert® a reservoir DDS which releases progesterone and acts as an intrauterine contraceptive. Drug eluting stents are coated in a drug-containing polymer is an example of a monolithic DDS. Transdermal patches are polymer DDS that adhere to the skin, these systems are designed to be either reservoir or monolithic. An example is the NICODERM® patch manufactured by Johnson and Johnson.

A potential drug for delivery is curcumin, it is selective in its apoptotic and non-proliferative effects. This is due to the phenotype of tumour cells. Firstly, it has been shown that tumour cells have increased uptake of curcumin [45], thus localizing its effects. Secondly, many tumour cells have constitutively activated NF-κB, a complex that regulates DNA transcription, which can result in cells proliferating uncontrollably. Curcumin acts to inhibit this over-activation, thus reducing proliferation [46]. Additionally, glutathione acts to reverse the inhibition of NF-κB by curcumin which would allow for proliferation. Lower levels of glutathione in tumour cells compared to healthy cells reduces that ability [47]. This selective capability would provide an additional means of targeting activity against tumour cells.

2.3. Common Fiber Production Methods

There is an extensive list of fiber production methods [48] which use a combination of principles covered below. However, for the purpose of this work, a brief summary of three methods will be covered with a focus on centrifugal spinning. Many of these

methods have been used for biomedical purposes such as tissue engineering and drug delivery.

2.3.1. Extrusion Fiber Production

Formation of fibers via extrusion require polymers to be in a viscous liquid state, typically achieved through melting for thermoplastic or by dissolving in a solvent for non-thermoplastic polymers. The liquid is then forced through a spinneret which contains pores, to form fibers. There are three main types of extrusion fiber formation: wet spinning, dry spinning and melt spinning. Wet spinning, uses solvents to both dissolve the polymer prior to extrusion and then to precipitate the fiber post-extrusion. Dry spinning, in contrast to wet spinning uses air or an inert gas to evaporate the dissolving solvent post-fabrication, resulting in solidification. Melt spinning, as its name suggests, is the melting of a thermoplastic polymer and cooling of the polymer post-fabrication which results in fiber solidification[48].

Melt spinning is unique in that it does not require the use of solvents. The use of solvents in some spinning methods carry concerns related to environmental impact, toxicity of final product and a decrease in productivity and efficiency of the overall process. Without the use of solvents in melt spinning the concern for solvent-related toxicity for biomedical applications and requirement of polymer solution concentration optimization for spinnability is eliminated, a notable advantage. Additionally, the solidification of fibers after extrusion involve a one-way heat transfer, a rapid process resulting in high production rates, in comparison to solution spinning which requires evaporation, a mass transfer which is less efficient [48].

Some biomedical applications of extruded fibers include, extruded collagen fibers as a scaffold for tissue engineering [49], microextruded polyesters for tissue engineering scaffolds and controlled drug delivery applications [50] and synthetic sutures that are extruded polymers which are sometimes further processed by braiding.

2.3.2. Electrospinning Fiber Production

Production of fibers via electrospinning involves polymers dissolved in an appropriate solvent which is fed through a needle with flow controlled by a syringe pump. A droplet is formed at the tip of the needle which is held in place by its surface tension. With an applied voltage between the needle and a grounded collector plate located some distance away from the needle, a charge is induced within the droplet. These charges repel each other within the droplet and at a critical point, this force will overcome the surface tension holding the droplet in place and a distortion, termed Taylor cone will form and a jet will exit this cone to form fibers. The fibers will travel towards the collector and while the solvent evaporates, the fiber undergoes a whipping motion resulting in elongation and a fiber diameter decrease. This method has several processing parameters which may be modified in order to optimize the fiber morphology desired. These include: needle-to-collector distance, viscosity of solution, polymer concentration, applied voltage, solution flow rate, electrical conductivity and the temperature and humidity of experimental space. These parameters allow for tailoring of fiber morphology. Diameters of fibers produced from this method range from tens of nanometers up to micrometers. These fibers have a large surface to volume ratio, an ideal property for many applications.

Examples of electrospun fibers used in the literature for biomedical applications include tissue engineering scaffolds for bone [51], neural [52], vascular [53] as well as other tissues. The versatility of electrospinning allows for a variety of materials to be spun into random and aligned fibrous mats. Electrospun fibers have also demonstrated utility as drug carriers, for example anti-virals were incorporated into electrospun cellulose acetate phthalate fibers as a means to deliver the drug and prevent transmission of the human immunodeficiency virus [54]. Electrospun fibers are of interest in manufacturing wound dressings given the potential of nanofiber mats mimicking the native extracellular matrix (ECM) structure of skin, encouraging innate repair systems to generate ECM components and encouraging repair of the

wound. In combination with the structure of the fibers, impregnation of drugs may further encourage repair through preventing infection with antibacterials or therapeutic agents known to improve repair [55]. Materials such as cellulose acetate phthalate [54], poly(lactic-co-glycolic acid) (PLGA) [56], and poly(caprolactone) (PCL) [57, 58] have been used for these applications.

2.3.3. Centrifugal Melt Spinning Fiber Production

Centrifugal melt spinning has been used for over 100 years in the form of a sugar spinning apparatus, also known as a cotton candy machine. It was invented and patented in 1897, at that time called an "electric candy machine" and in 1904, cotton candy was introduced at the St. Louis World Fair. Since 1897, cotton candy production has been rather unchanged [59]. Sugar is loaded into a reservoir made of a heat conductive material where it is melted, the reservoir contains small openings called orifices. The term spinneret is used to label the reservoir and its orifices **(Figure 2.4)**.

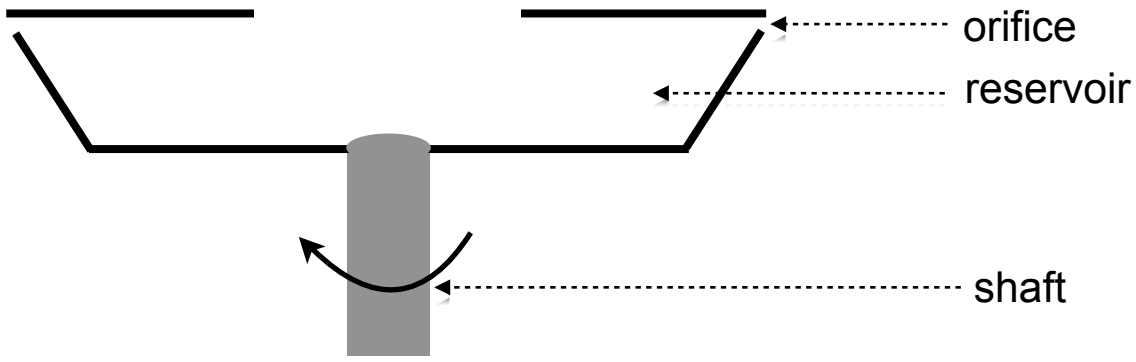

Figure 2.4: A general schematic of a spinneret illustrating the reservoir, orifices and the mounted shaft.

The spinneret rotates about its axis, above a heating element which melts the loaded material, fibers leave the orifice and are collected. The centrifugal force due to the rotation forces the material to exit the orifices and as that force overcomes the surface

tension of the material at the orifice a polymer jet is forms, the fiber solidifies rapidly in the air and deposits onto the collector.

This rapid method of fiber production has been utilized by a relatively small number of research groups. Badrossamay *et al*. [60] first published their work in 2010 using the principles of a cotton candy machine to solution spin nanofibers. They termed the method rotary jet spinning (RJS). This method was able to produce aligned poly(lactic acid) (PLA) nanofibers ranging from 50-3500 nm in diameter for the guidance of rat cardiomyocytes. The range of fiber diameters produced was wide and dependent on the rotation speed of the spinneret. In 2014, the group published work with polymer-protein hybrid, poly(caprolactone)(PCL) and collagen or gelatin. This work utilized the same fiber production method (RJS) and were successful in producing highly aligned nanofibers for the purpose of influencing cell migration [61]. Since then, this method has become of increasing interest in the field for tissue engineering [58] and this interest may be further increased with the availability of a commercial centrifugal spinning machine from the company FibeRio, based on the patented Forcespinning ® technology for producing nanofibers [62]. One of the main advantages of a centrifugal fiber production method is the low cost and high yield [63]. Although there are some limitations associated with this method such as constraints due to the materials' properties resulting in variable fiber quality and morphology [48]. An additional limitation is the ability to align the fibers has been shown to be unidirectional. However, it has been noted that for tissue engineering applications, control of lamination to mimic native extracellular matrices is highly sought after [64] and this has not been demonstrated with centrifugal spinning.

2.4. Materials for Fiber Spinning

Various materials have been used for fiber spinning with applications ranging from textiles and insulation to the biomedical industry, of which biomaterials are a major component. Biomaterials encompass materials which are in contact with biological systems. There are various polymer options for these materials which may be tuned to

have appropriate chemical, physical and biological properties. Proper selection of appropriate polymers and modifications are essential to a biomaterials' performance. For example, a biomaterials' surface topography, size and shape can affect the host response and if mismatched, can result in infection, fibrosis and poor performance of the material.

2.4.1. Polymers

The use of natural polymers for biomaterials possesses the advantage of biocompatibility and bioactivity due to their innate function in the body, these materials include collagen, chitosan and silk fibroin. In particular, collagen forms the extracellular matrix of many tissues in the body, aiding in the maintenance of structural integrity and playing an integral role in cell signalling. Collagen has been used to produce fibers for tissue engineering applications. These fibers possess many attractive properties including: low antigenicity, good cell compatibility, low cytotoxicity and biodegradability. However, a downfall of collagen is the low availability of human sources. Most commonly used collagen sources are porcine, bovine and equine. The use of non-human collagen may lead to deficiencies in biomaterial performance due to the heterogeneity, untraceable origins, the possibility of disease [65] or immunological stimulator transmittance [66]. Recently, the advent of human recombinant collagen production provides the possibility of using human-only sources for applications [67].

Alternatively, synthetic polymers are often used in biomedical research given their availability and potential for simple modification and functionalization. They can be categorized broadly into hydrophilic and hydrophobic polymer based on the properties of their monomer units. Common hydrophobic polymers used for biomedical applications include, poly(caprolactone) (PCL), poly(ester amide) (PEA) and polydimethylsiloxane (PDMS). Common hydrophilic polymers are poly(ethylene glycols)(PEG), poly(ethylene oxide)(PEO) and poly(vinyl alcohol)(PVA).

Another consideration about polymers is their hydrophilicity. Hydrophilicity of a polymer is determined by the functional groups it possesses such as hydroxyls, carboxyls, carbonyls, amines and amides and their interaction with water molecules through hydrogen bonding. Increased hydrophilicity will result in increased and stronger interactions with water and swelling of the material resulting in changes in mechanical and chemical properties [68]. Effects due to the hydrophilicity of a material can influence cell adhesion [69], increase water absorption, have anti-fouling properties[70] and enhance drug solubility and thus drug delivery.

2.4.2. Poly(ethylene oxide)

Poly(ethylene oxide) (PEO) is a synthetic crystalline, thermoplastic and water-soluble polyether compound **(Figure 2.4)**, these compounds are called poly(ethylene glycol) (PEG) or PEO depending on their molecular weight, PEO for the higher molecular weights. The threshold for naming varies in the literature with values of 10 000 g/mol [71] and 25 000 g/mol [72] reported. PEG and PEO are commonly used for biomedical purposes as a conjugate for increasing solubility of hydrophobic drugs [73], coating of materials to prevent protein adsorption and opsonization [74] which could stimulate the immune system and result in immune system attack and immune rejection. These applications exploit the hydrophilicity of PEG and PEO to avoid these complications.

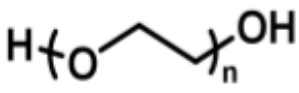

Figure 2.5: Chemical structure of PEG and PEO, where n is the number of monomer units.

Many modifications of PEO have been studied in the field of biomedical engineering. With hydroxyl end groups and high solubility in organic solvents, end-group modifications are relatively simple and the polymer may undergo a variety of

reactions. Copolymerization of PEO to other polymers to impart distinct properties such as flexibility and hydrophilicity has been shown to be effective [75]. Imparting properties of PEO may allow for materials typically involved in protein adsorption to resist such interactions and reduce the risk of undesirable biological responses such as clotting [76]. In addition to copolymerizing PEO in a linear fashion, PEOs have been polymerized in star shapes [77, 78], a form of branching. The ability to tailor the shape of polymer branching allows for tuning of properties such as viscosity [79], porosity of constructs [78] and stimuli-sensitivity [80] for the desired application. PEO is a versatile, FDA approved polymer currently used in cosmetic and pharmaceutical products [81, 82] due to its non-toxicity and effective clearance through urinary and fecal excretion [75].

2.5. Crosslinking Options for Polymers

Water-soluble polymer fibers such as PEO fibers must undergo post-processing modification to stabilize them in aqueous environments such as body fluids. Intermolecular bonds may be formed in order to create insoluble networks. The degree of crosslinking which is related to stability and biodegradation may be tailored depending on the particular application.

2.5.1. Methods of Crosslinking

The two main methods for crosslinking of polymers are chemical and physical. Chemical crosslinking involves the addition of a chemical group to join molecules together. Examples include genipin which may react with amine groups of proteins such as collagen [83] and polysaccharides such as chitosan [84]. Similarly, glutaraldehyde and formaldehyde react with hydroxyls of many different polymers and link molecules together through those newly formed covalent bonds. Physical crosslinking methods use the addition of energy through changes in temperature such as thermal cycling, through UV light for photocrosslinking and also through high energy ionizing radiation such as ion beam implantation or x-ray which form free

radicals which reform into crosslinks. Physical crosslinking is often preferred for biomedical applications as they do not introduce new chemicals into the final product. However, chemical crosslinking methods are highly effective and if removal of free reagents is possible and the byproducts of degradation are non-toxic this method is useful [85].

2.5.2. Photochemical Crosslinking

For this work, the use of photochemical crosslinking was employed. This method involves the addition of a chemical group to render the polymer sensitive to UV light. After the addition of this carbon-carbon double bond, the exposure to UV light results in radical formation and bond reformation between functionalized chains resulting in a network of crosslinked molecules (**Figure 2.6**) [86]. A downside of this method is the requirement of two separate steps, functionalization followed by photocrosslinking with UV irradiation. However, a benefit would be the ability to tune both the extent of functionalization as well as length of irradiation time to tune the degree of crosslinking.

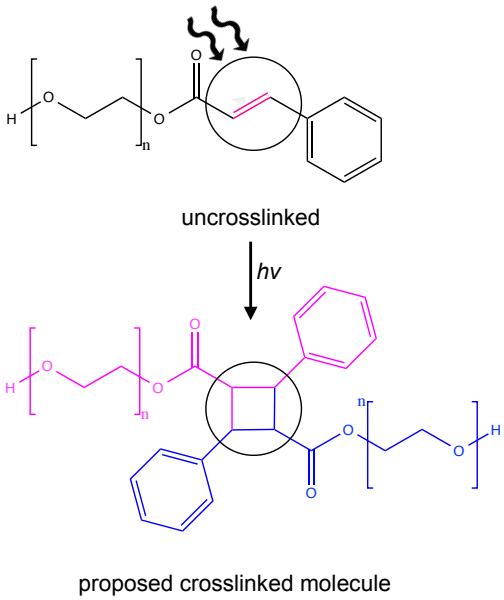

Figure 2.6: Proposed crosslinked molecule of PEO-cinnamate after UV irradiation.

2.5.3. Cinnamoyl Chloride

Cinnamate functionalized polymers have been used extensively for biomedical research purposes. Photocrosslinking of electrospun fibers post-production [87] and *in situ* during electrospinning have been performed [88]. Cinnamate modified polymers have been shown to undergo UV crosslinking via [2+2] photocycloaddition [86]. As an acid chloride, cinnamoyl chloride is a highly reactive molecule in comparison to its carboxylic acid counterpart due to the chloride being an excellent leaving group and will readily undergo nucleophilic reactions. This allows for efficient functionalization of polymer end-groups. Reactions involving cinnamoyl chloride should be performed under dry conditions given that cinnamoyl chloride is highly reactive with water and would render the molecule less reactive once converted to cinnamic acid.

Cinnamic acid has a natural origin, and is widely present in the plant kingdom, in particular in the essential oils of basil and cinnamon [89]. Cinnamoyl chloride, modified from cinnamic acid is typically used to functionalize polymers, there is potential for cinnamic acid to form during ester hydrolysis of the crosslinks. Fortunately, there is no evidence to support that this molecule possesses a toxic threat [89, 90]. Cinnamoyl chloride has been shown to have low toxicity as it is spontaneously metabolized in the body [91]. And is thus a good option for crosslinking water-soluble polymers for biomedical applications.

2.6. Assessment of Delivery Systems

2.6.1. Drug Efficacy and Cell Compatibility

Evaluation of a drug's effectiveness as delivered from the drug delivery device is an integral step in demonstrating design and production accomplishments.

Determination of a drug’s efficacy is typically performed prior to the design of a drug delivery device as DDS are used to improve on pre-existing drugs. Tests performed to

evaluate a drug's performance include assays to determine the effective concentrations (EC) for agonists and inhibitory concentrations (IC) for antagonist drugs. EC50 and IC50 values are defined as the drug concentrations that exhibit 50% of *in vitro* response (**Figure 2.7**). These values may be used in the classification of drugs for their potency and the plots of activity may be guidelines for dosing.

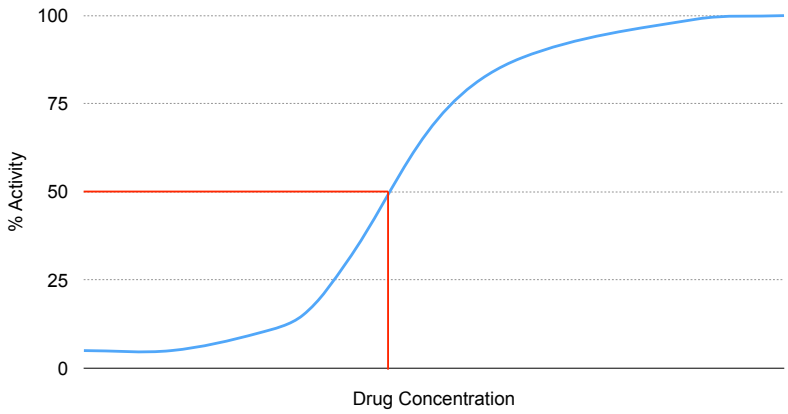

Figure 2.7: Definition of IC50/EC50 graphically, drug concentration at 50% activity is defined as the IC50/EC50

The selection of an appropriate cell line involves the consideration of several variables such as the cell species as some studies are species-specific and also the functional characteristics of interest for the experiment such as surface and intracellular targets. For testing of pharmacological agents, understanding the cellular targets of the drug may guide selection of the cell line for testing. For study of cancer cells in particular, the source of the cells is not the only variable to consider given that cell lines mutate and do not necessarily represent the cancer from which it was sourced as a whole. Selection of cell lines based on cellular targets and ensuring the drug acts on those targets will provide valuable information for translating into *in vivo* studies. Cancer cell lines do not necessarily represent the heterogeneity of tumours and thus a gap exists between *in vitro* studies and clinical samples [92].

2.6.2. Appropriate Evaluation of Transdermal Drug Delivery

In addition to evaluating DDS *in vitro*, studies with appropriate animal models is integral prior to clinical studies. The purpose of animal studies is to evaluate the efficacy and safety of the proposed system. Focusing on transdermal drug delivery, the assessment of delivery through the skin is a major step in evaluating the system. It is nearly impossible to assess skin permeation using just one assessment either *in vitro*, *in vivo* or *ex vivo* [93]. Thus, a combination of these experiments is required for effective demonstration of delivery. For these assays, human skin is the most relevant for study, however availability may be limited. An animal model that is appropriate for study will have similar structures when compared to human skin, possessing similar density of hair follicles, thickness of epidermis and dermis. Animal models suggested include primate, porcine, snake and rodent. For some of these animals, considering a hairless counterpart maybe be beneficial as they are better representations of humans [93].

In addition to studying drug permeation, animal models with representative disease states will be of importance to demonstrate the drug permeation and activity of the drug. For skin cancer, nude rodent models with established protocol for inducing UV skin damage have been proposed [94].

3. HYPOTHESIS AND OBJECTIVES

3.1. Hypothesis

Firstly, we hypothesize that poly(ethylene oxide) (PEO), a biocompatible polymer can be modified and processed into stabilized microfibers. Since PEO is water-soluble and the fibers will be in contact with bodily fluids, aqueous stability must be imparted through crosslinking using cinnamoyl chloride (CC), a highly reactive acyl chloride to introduce an ultraviolet (UV) sensitive double bond to the polymer for photocrosslinking. Secondly, we hypothesize that these stabilized fibers will be able to carry and deliver curcumin at a sustained level sufficient to inhibit cell proliferation and promote cell death.

3.2. Objectives

This work aims to study the potential of a crosslinked polymeric fiber system for carrying and delivering curcumin and demonstrating the efficacy of curcumin on a cancer cell line. The main objectives of this work are to:

1. Synthesize an ultraviolet (UV) sensitive polymer by functionalizing poly(ethylene oxide) (PEO) with cinnamoyl chloride.
2. Using this bulk material to produce microfibers using centrifugal melt spinning.
3. UV irradiation of the fibers to crosslink the polymer at cinnamoyl moieties.
4. Investigate curcumin loading and release from crosslinked, stabilized fibers.
5. Study the effects *in vitro* of free curcumin and curcumin from loaded PEO-cinnamate fibers.

Ultimately the goal is that centrifugal melt spun PEO-cinnamate fibers will carry and release curcumin locally at the site of precancerous lesions.

4. MATERIALS AND METHODS

4.1 Materials

Table 2: Materials for experimental procedures

Material	Supplier	Detail	Item Number
Poly(ethylene oxide)	Sigma Aldrich	35 000 g/mol	25322-68-3
trans-Cinnamoyl chloride	Alfa Aesar	97% purity	17082-09-6
Curcumin	Sigma Aldrich	≥94% curcuminoid content	458-37-7
Anhydrous ethyl alcohol	Commercial Alcohols	99.8%	Lot # 018568
Dichloromethane		Solvent purification system, Dept. of Chemistry, UWO	
Pyridine	Sigma Aldrich	Anhydrous, 99.8%	270970
Phosphate Buffered Solution	Sigma Aldrich	Tablets	P4417
AMEM-alpha	Wisent Inc.	+ 10% FBS	310-022-CL
Trypsin-EDTA	Wisent Inc.	0.25% trypsin	325-043-EL
Phosphate Buffered Solution	Gibco	(-) $CaCl_2$, $MgCl_2$	10010-023

4.2. Synthesis: Functionalization of Poly(ethylene) oxide with Cinnamoyl Chloride

100 g (2.857 mmol) of PEO was frozen in a -20 °C freezer then subsequently lyophilized. The samples were freeze-dried for 18 hours at 0.04 mbar at -180 °C. Lyophilized PEO was dissolved in 400 ml of dry DCM under stirring. An additional 300 ml of molecular sieve dried DCM was added. Next, 3.5 ml (0.035 mmol) of dry pyridine was added. Subsequently, 5 g (30 mmol) of cinnamoyl chloride was added

and the reaction vessel was covered entirely with aluminum foil to protect from photo-damage. The reaction proceeded under the following conditions: room temperature, constantly stirred at 400-600 RPM and under a N_2 atmosphere for approximately 24 hours. After which, PEO-cinnamate was precipitated, 2 L of diethyl ether was used to precipitate each 100 ml volume of PEO-cinnamate dissolved in DCM. The solution of of DCM and PEO-cinnamate was manually poured, slowly, into a beaker of magnetically stirred diethyl ether (500 RPM). The precipitate was then isolated using vacuum filtration and desiccation at room temperature for a minimum of 48 hours, covered entirely with aluminum foil to protect from potential photo-damage. PEO-cinnamate remained under house vacuum until further processing was required. The synthesized product along with the reactants, PEO and cinnamoyl chloride then underwent differential scanning calorimetry (DSC), Fourier Transform Infrared Spectroscopy (FTIR) and proton nuclear magnetic resonance (^{1}H-NMR) for characterization.

4.3. Chemical Characterization

4.3.1. DSC

Differential scanning calorimetry (DSC) analysis of cinnamoyl chloride, PEO and PEO-cinnamate was performed using a TA instruments Thermal Analysis DSC at a heating rate of 10 °C/min under nitrogen. The melting points were determined from the second heat scan at the peak point of the thermograms.

4.3.2. FTIR

A Bruker spectrophotometer was used to obtain FTIR spectra of solid samples of cinnamoyl chloride, PEO, PEO-cinnamate and crosslinked PEO-cinnamate with and without curcumin.

4.3.3. ^{1}H-NMR

^{1}H-NMR analyses of cinnamoyl chloride, PEO and PEO-cinnamate were performed

using a Varian Inova 600 spectrophotometer. Spectra were obtained in $CDCl_3$ at 600 MHz. The percentage of functionalized PEO was determined my integration of signal strengths at 3.65 ppm and 6.50 ppm associated with PEO non-hydroxyl hydrogens and cinnamate alkene hydrogen adjacent to the ester, respectively.

4.4. Centrifugal Melt Spinning

Fibers were produced using a modified cotton candy machine (Sanrio, Hello Kitty, Model: #APP-96209) shown in **Figure 4.1**. The cotton candy machine was modified with the replacement of the motor, with a 250 W brushless DC motor and EPOS2 70/10 controller purchased from Maxon Motor (Switzerland). Additionally, a 48 V, 600 W power supply from Mean Well (USA) was added. Fibers were produced with the as-purchased system as well as with modifications and designed spinneret **(Figure 4.2)**.

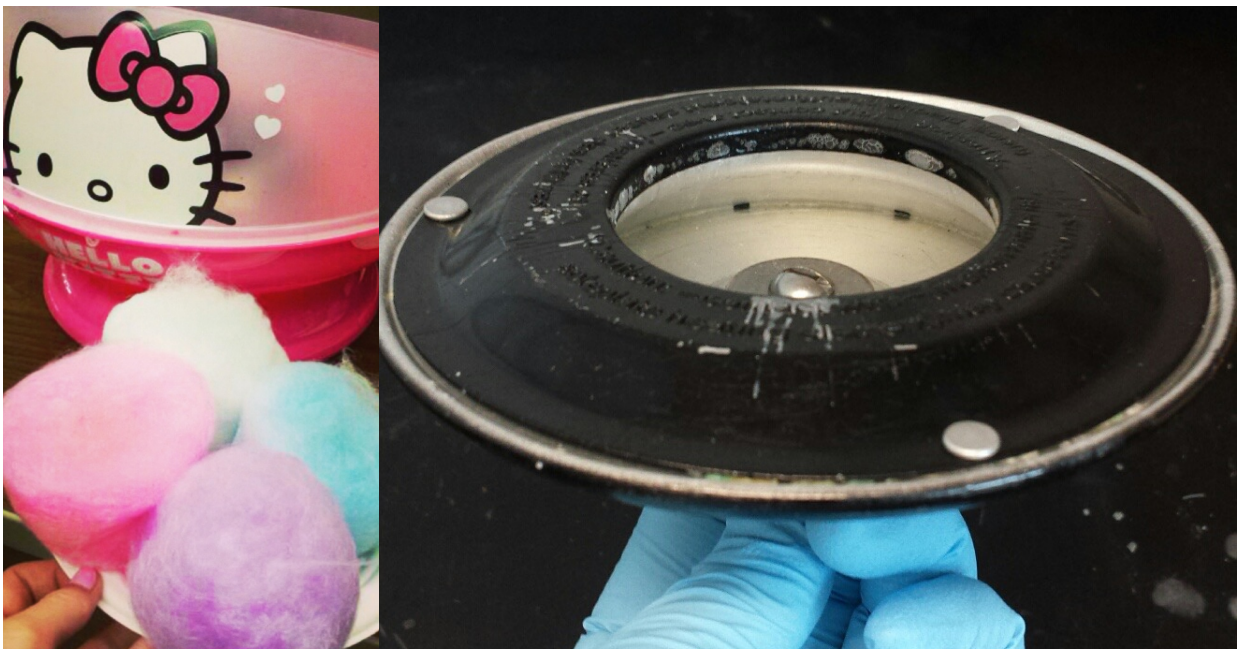

Figure 4.1: Hello Kitty Cotton Candy Machine as-purchased with first batched of spun sugar (**left**). Spinneret of as-purchased system (**right)**.

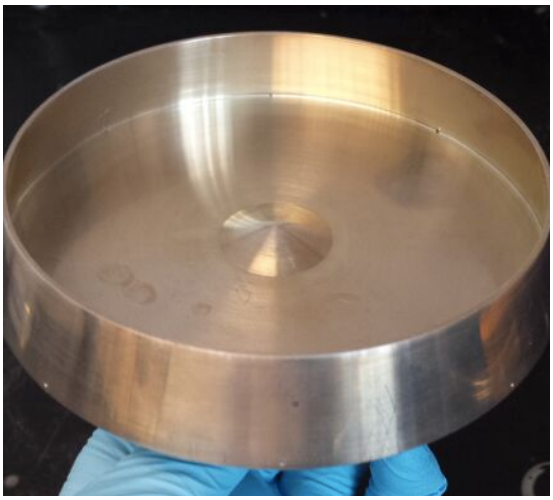

Figure 4.2: New spinneret design for the modified cotton candy machine.

4.5. Fiber Characterization and Image Analysis

4.5.1. Scanning Electron Microscopy

A Hitachi S-3400N variable pressure scanning electron microscope was used to obtain high resolution images. Nine locations were pre-selected using accompanying software to allow for consistency between samples. An accelerating voltage of 10 kV and working distance of 21 - 25 mm was selected.

4.5.2. Image Processing

ImageJ was used to measure and collect fiber diameters from SEM images. Scale bars located at the bottom right corner of each SEM image was used to calibrate the measurement tool and fiber diameters were measured perpendicularly to fiber edges.

4.6. UV Crosslinking and Characterization

4.6.1. UV Irradiation

PEO-cinnamate fiber samples were irradiated by with UV for various lengths of time at a distance of 5 cm from the light source **(Figure 4.3)**. UV/Vis was performed as described below.

4.6.2. UV/Vis

A Beckman Coulter DU520 General UV/Vis spectrophotometer was used to obtain UV/Vis spectra. Fiber samples were suspended in deionized water in a quartz cell and thin films were cast onto quartz slides and dried prior to measurements for UV-crosslinking studies. Absorbances at λ=277 nm were obtained.

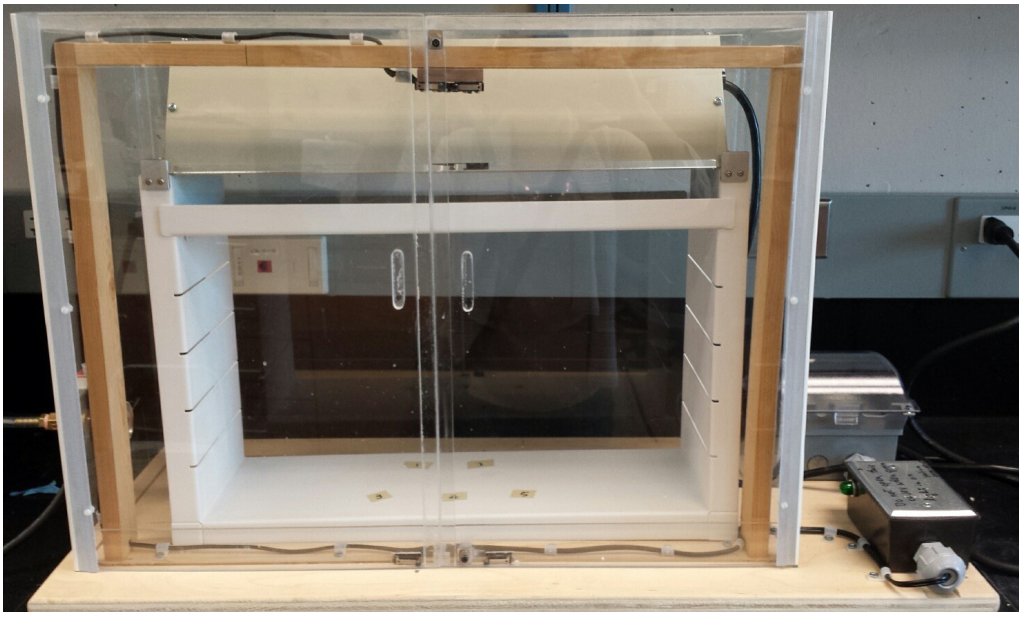

Figure 4.3: UV lamp for sample photocrosslinking with shelf set at 5 cm from lamp.

4.7. Curcumin Loading and Characterization

4.7.1. Loading Procedure

Crosslinked PEO-cinnamate fibers were covered with 5 ml of an ethanol and curcumin solution and allowed to soak for 24 hours. After which, samples were centrifuged at 6000 RPM for 15 minutes, the supernatant was removed and fibers were washed with a series of water and EtOH solutions, diH_2O x 1, 50% ethanol/ diH_2O x 1 and diH_2O x 1, after each wash, samples were centrifuged at 6000 RPM for 5 - 10 minutes. After the final water wash and supernatant removal, remaining diH_2O was left with the fibers overnight. After 24 hours, diH_2O was added for a final wash prior to release studies.

4.7.2. Loading Efficiency

Curcumin loading efficiency was determined by repeatedly washing loaded samples in 10 ml of ethanol, centrifugation to isolate fibers until curcumin was no longer detectable in the supernatant. The ethanolic supernatant was sampled and analyzed using UV/Vis spectroscopy. The values were compared to a standard curve of curcumin in ethanol. Absorbances at λ=427 nm were obtained.

4.8. Curcumin Release

Loaded curcumin fibers were placed into 5 ml of phosphate buffer solutions (PBS) with a pH of ~7. Release was monitored over a period of 14 days. The centrifuge tubes were centrifuged at 6000 RPM for 12 minutes, and the supernatant was collected at specific time points. Samples were analyzed using UV/Vis spectroscopy.

4.9. Cell Studies

4.9.1. Cell Culturing

A549 human lung carcinoma cells were maintained at 37°C and 5% CO_2 in Minimum Essential Medium Alpha Medium (AMEM, Wisent Inc.) supplemented with 10% fetal bovine serum (FBS, Wisent Inc.). Dose-response curves were determined by incubating $1x10^5$ cells/flask (T25, Nunc™ Thermo Scientic) with various concentrations of prepared free curcumin solutions with final concentrations in culture media of 0, 0.5, 1, 2, 5, 10, 15, 20, 50 and 100 μM for the first trial and 0-10, 12 and 15 μM for the final two trials. Three replicates were used per treatment group.

4.9.2. Free Drug Solution Preparation and Measurement

Curcumin was dissolved in ethanol and serially diluted to achieve the above concentrations (**4.9.1.**). This was completed under non-sterile conditions thus sterilization was required prior to treating the cells. Under sterile conditions, solutions were subsequently filtered through 0.2 μm syringe filters to remove potential bacteria, fungal spores and undissolved particles of curcumin. To ensure accurate

concentrations produced after filtering, a volume of curcumin solution was removed and UV/Vis spectroscopy was used to measure absorbance and compared to a standard curve to determine curcumin solution concentrations.

4.9.3. Cell Proliferation Determination

After 72 hours of incubating with free curcumin, media was removed, cells were rinsed with PBS, trypsinized with 0.5 ml trypsin-EDTA and diluted with 19.5 ml of PBS for cell counting. A Beckman Coulter Counter was used for cell number determination. Two counts were performed per flask of cells and the average was used. A fresh vial of cells was thawed for the last dose-response experiment.

4.10. Statistical Analysis

Statistical analysis was performed using GraphPad Prism™ version 5.0c.

5. RESULTS AND DISCUSSION

This chapter begins with the synthesis and characterization of PEO-cinnamate to functionalize PEO with a carbon-carbon double bond for UV photocrosslinking (Section 5.1). Cinnamoyl chloride was selected to add a photocrosslinkable functional group to the water soluble polymer PEO as it was previously demonstrated to be an effective molecule with no known toxic effects [89]. The utility and spinneret parameters of centrifugal melt spinning for the production of PEO-cinnamate fibers were investigated through observation and measurement of fiber morphology and diameter (Section 5.2).

The material selected for producing the fibers is PEO, for its biocompatible and hydrophilic properties, as-spun, these fibers are not stable in aqueous environments. PEO-cinnamate as spun fibers are also not stable in aqueous environments. For the stabilization of fibers for contact to aqueous environments, such as *in vitro* and *in vivo*, a UV photocrosslinking treatment is used (Section 5.3).

For the purpose of drug delivery, curcumin was loaded into the stabilized fibers via diffusion and the relationship between the loading concentration of curcumin and amount of loaded curcumin was determined (Section 5.4). The release of curcumin from the system in PBS was observed for 2 weeks to study the release kinetics (Section 5.5).

To begin the assessment of the system, a free curcumin dose-dependence curve was determined with the human A549 cancer cell line (Section 5.6). This will allow for comparison to similar curcumin doses released from fibers.

Figure 5.0 is a flow chart to outline the contents of this chapter.

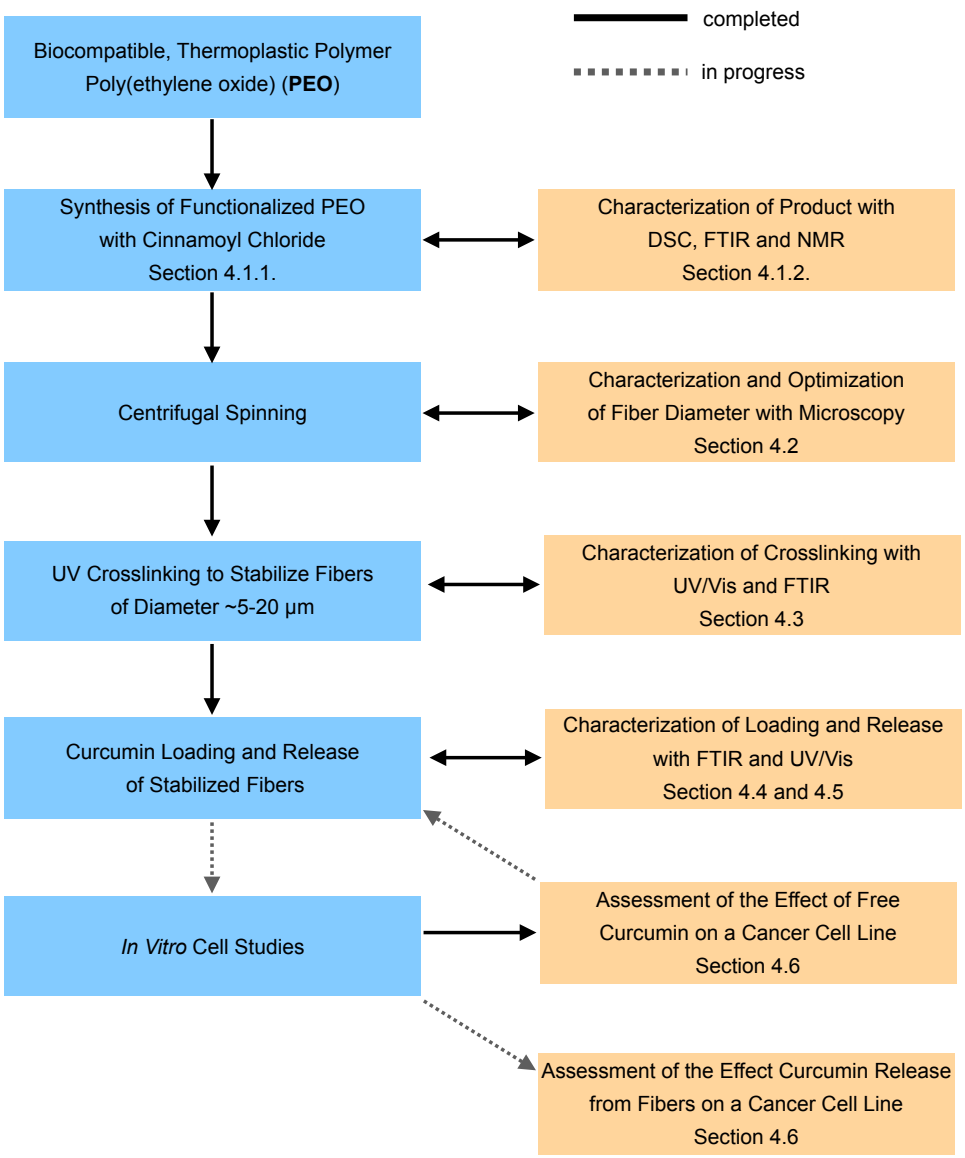

Figure 5.0: Flow-chart outlining contents of this chapter.

5.1. Synthesis and Chemical Characterization of Polymer

5.1.1. Synthesis of PEO-cinnamate

PEO-cinnamate was synthesized by functionalizing PEO with cinnamoyl chloride via an esterification reaction involving the hydroxyl groups of PEO and the reactive acyl chloride of cinnamoyl chloride with the presence of pyridine for deprotonation of PEO hydroxyls **(Scheme 5.1)**. The product was then precipitated in diethyl ether, isolated and purified through vacuum filtration and diethyl ether rinsing and finally dried under house vacuum.

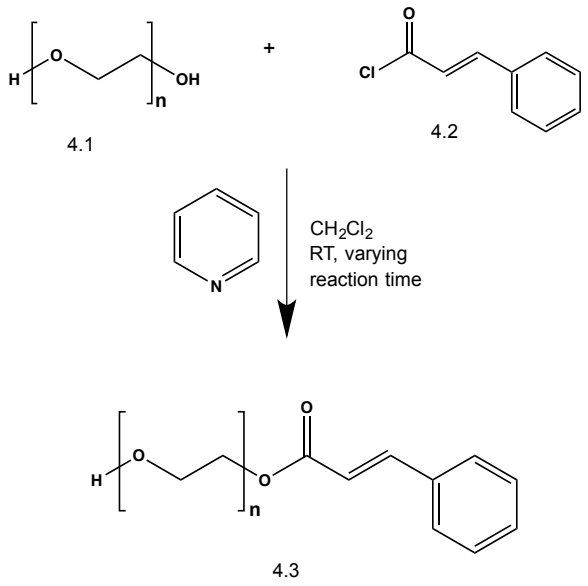

Scheme 5.1 - Deprotonation of PEO (4.1) by pyridine followed by esterification with cinnamoyl chloride (4.2) to form PEO-cinnamate (4.3).

5.1.2. Chemical Characterization of Product

To demonstrate functionalization of PEO with cinnamoyl chloride, differential scanning calorimetry (DSC) was performed on the reactants and product of the synthesis reaction. DSC spectra show distinct single peaks for reactants and product. Melting temperatures for cinnamoyl chloride, PEO and PEO-cinnamate are 32°C, 66°C and 61°C, respectively **(Figure 5.1)**. The product has an intermediate melting

temperature demonstrating functionalization and the sharp single peaks demonstrate purity of the reactants and product.

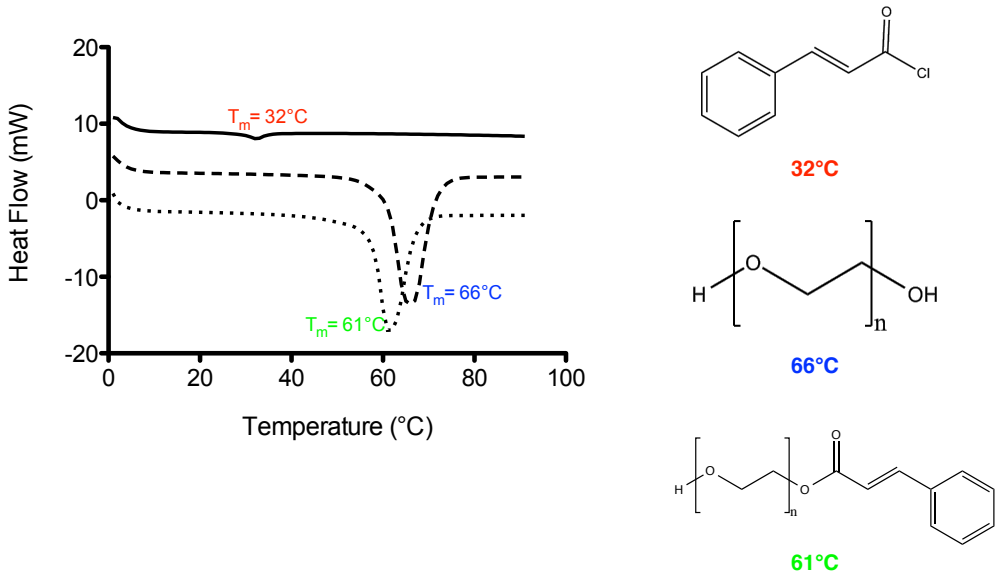

Figure 5.1: DSC thermograms of cinnamoyl chloride, PEO and PEO-cinnamate.

Demonstrating the purity of the end product, meaning no residual free PEO or cinnamoyl chloride shown with a single peak in the DSC thermogram is important in the step of characterization. Although, cinnamoyl chloride has been shown to be non-toxic *in vivo* [95].

Up until this point, the functionalization of PEO has been presented as a one-sided reaction. However, considering the symmetry of PEO's structure, there are three possible scenarios for this functionalization reaction. 1) unreacted, pure PEO (4.1), 2) single-sided functionalization (4.3) and 3) double-sided functionalization (4.4) **(Figure 5.2)**. Although, having unreacted PEO is highly unlikely due to the reactivity and use of excess cinnamoyl chloride. The possibility of multiple end products require the processing and interpretation of FTIR and ^{1}H-NMR spectra to take this into account.

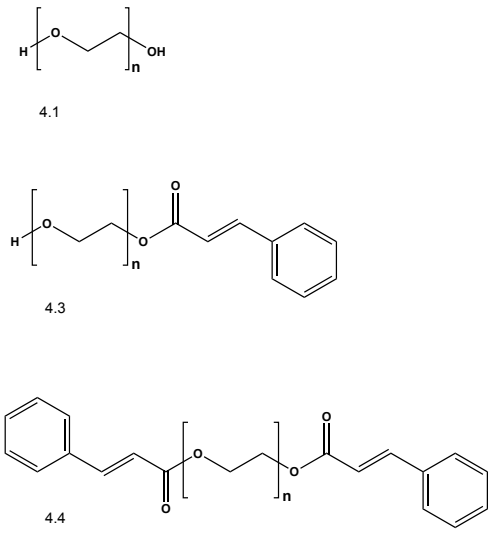

Figure 5.2: Chemical structures of possible outcomes of the synthesis reaction.

Next, FTIR was performed again on the reactants and product. The FTIR spectra of PEO shows an -OH stretch present in the 3600 cm^{-1} region and a strong sp^3 C-H peak in the 3000 - 2840 cm^{-1} region (**Figure 5.3**). These peaks are in agreement with the chemical structure of PEO. The FTIR spectra of cinnamoyl chloride shows a strong aromatic C=C stretch in the 1660 - 1500 cm^{-1} region and the strength of the peak can be attributed to the conjugation of the aromatic ring (**Figure 5.4**). Finally, the FTIR spectra for PEO-cinnamate shows a strong sp^3 C-H peak in the 3000 - 2840 cm^{-1} region comparable to the peak in PEO, however, there is no -OH stretch detectable, indicating two-sided functionalization through the disappearance of this peak when reacted with cinnamoyl chloride (**Figure 5.5**). Other peaks such as C=O and C=C detected in the cinnamoyl chloride spectra are not clear in the PEO cinnamate spectra due to the molecular size of the PEO polymer.

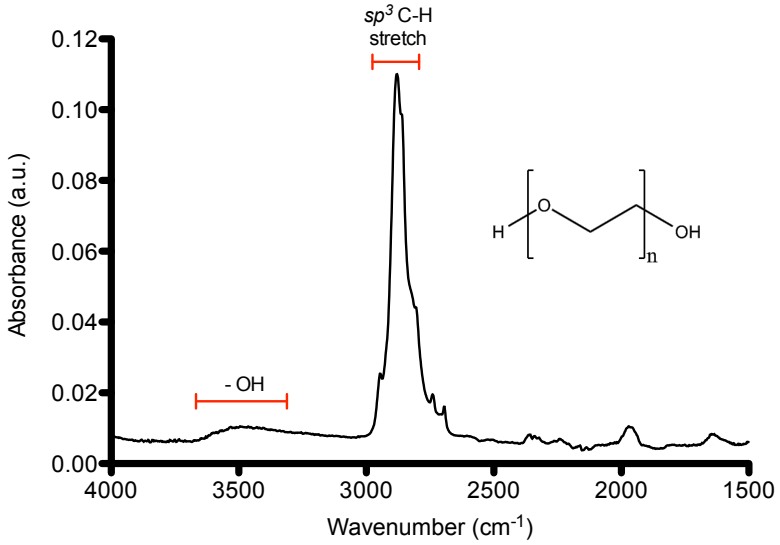

Figure 5.3: FTIR spectra of PEO. An *sp*^{3} C-H stretch predominates and a -OH is visible.

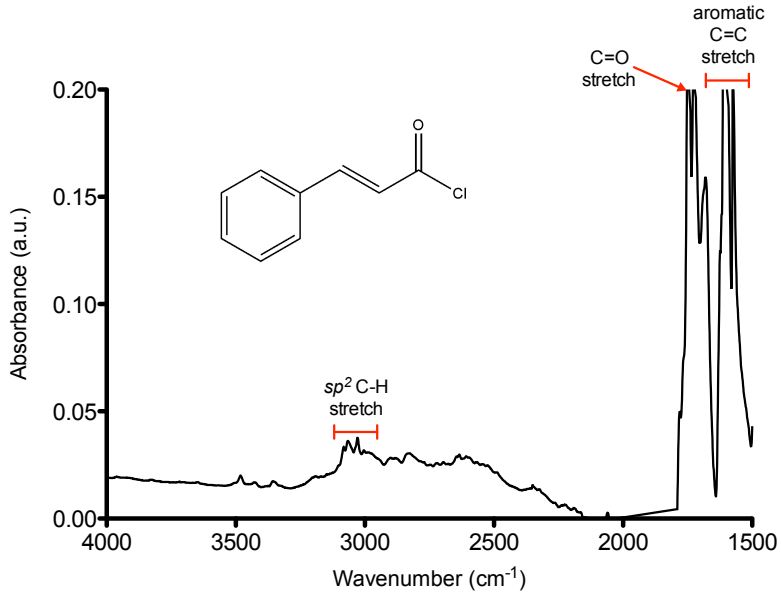

Figure 5.4: FTIR spectra of cinnamoyl chloride. Aromatic C=C stretch, C=O stretch and *sp*^{2} C-H stretch are present.

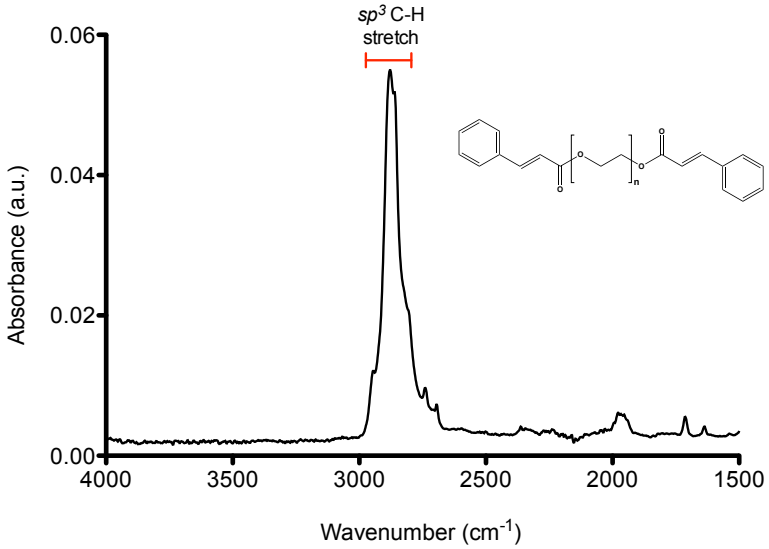

Figure 5.5: FTIR spectra of PEO-cinnamate functionalized on both ends. An sp^3 stretch is present and the -OH stretch is absent as compared to the PEO spectra.

To further characterize the product, ^{1}H-NMR was performed, and the functionalization of PEO with cinnamoyl chloride appeared successful, as evidenced by the shift in functionalized cinnamoyl peaks from 6.63, 6.66, 7.44, 7.48, 7.56, 7.82 and 7.85 ppm **(Figure 5.6A)** for free cinnamoyl chloride to 6.45, 6.48, 7.38, 7.44, 7.52, 7.68 and 7.71 ppm for functionalized cinnamate **(Figure 5.6B)**. The peaks are further downfield for cinnamoyl chloride compared to PEO-cinnamate due to the highly electronegative chlorine atom in cinnamoyl chloride which attracts the electrons surrounding each proton and results in less shielding and an increase in chemical shift.

Complete functionalization was achieved as determined by integration of the PEO multiplet at 3.65 ppm with respect to the doublet at 6.50 ppm associated with the hydrogen adjacent to the ester carbonyl of cinnamate (**Figure 5.7**). Additionally, there was no free cinnamoyl chloride as determined by the absence of those peaks **(Figure 5.6A)**.

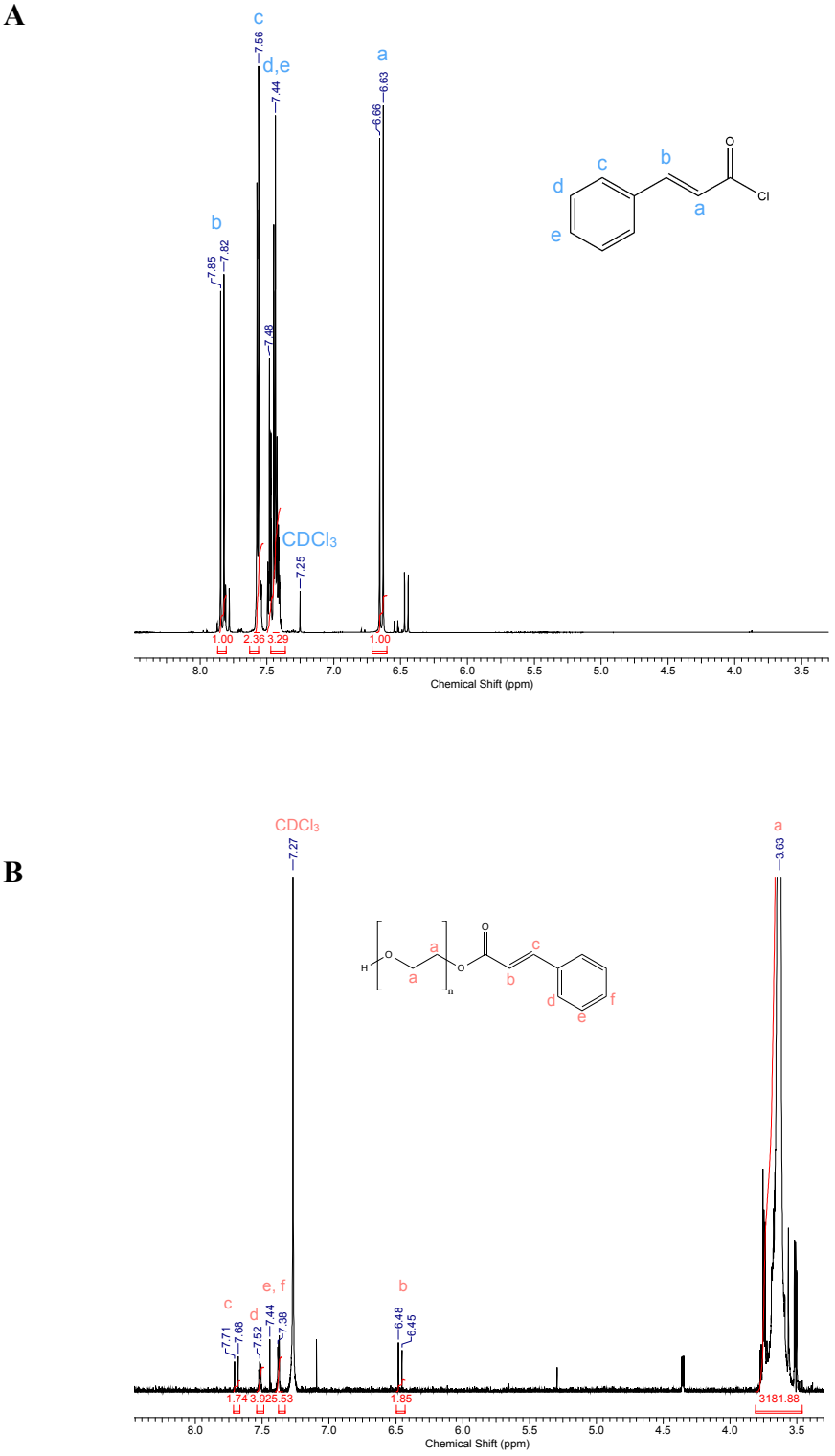

Figure 5.6: NMR spectra of pure cinnamoyl chloride (A) and the synthesis product and chemical structure of PEO-cinnamate (B). A chemical shift difference between pure cinnamoyl chloride and functionalized PEO-cinnamate is present.

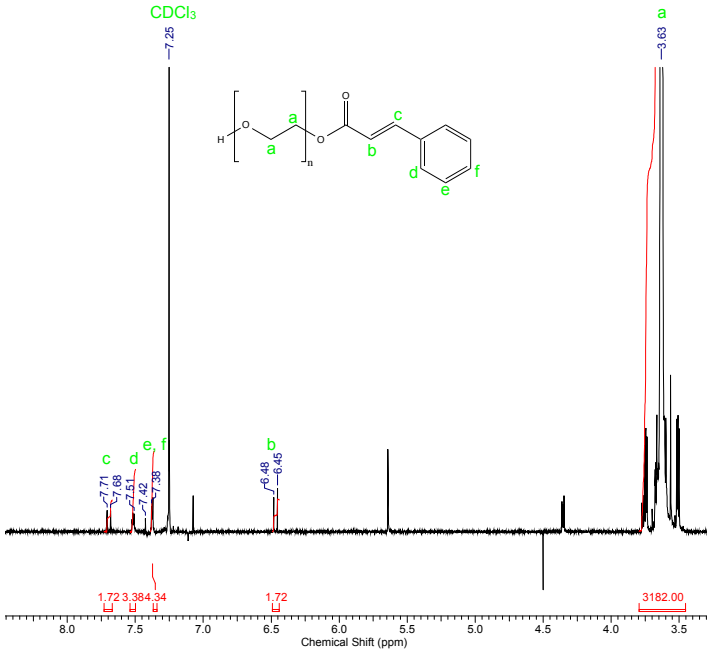

Figure 5.7: NMR spectra comparison of 4 hour (**5.6B**) and overnight (**above**) reaction times.

There is more than one way to process NMR data in terms of which peaks to set as the reference for integration. For instance, any of the peaks could be set as the reference if their value was known to be accurate. In this case, the PEO peak could be set as the reference as the number of hydrogens of a 35 000 g/mol molecule could be calculated with reasonable accuracy as determined by the supplier. With this method, after reaction times of 4 hours, 6 hours and overnight, 81.0 - 92.5% of the PEO hydroxyls were functionalized with cinnamoyl chloride on two sides as suggested by the integration value between one and two for the reactions. And 100% of molecules had at least one side functionalized.

This result also indicates that the shortest reaction time between PEO and cinnamoyl chloride of 4 hours is a sufficient amount of time to allow the reaction to proceed to completion. In the future, further optimization could be performed to further reduce this reaction time if desired. Another consideration would be the base used in

deprotonating the hydroxyls of PEO. A stronger base could make the reaction proceed at an even more efficient rate. However, with a stronger base such as triethylamine (TEA) an acid/base wash may be required to remove the excess base adding another step in the procedure.

These results reiterate the DSC and FTIR findings that PEO has been fully functionalized with cinnamoyl chloride and that a pure product is possible to obtain.

5.2. Characterization of Functionalized Fibers

In order to demonstrate the utility of a cotton candy machine for the production of fibers as reported by other groups, we produced pure PEO fibers using an as-purchased cotton candy machine and observed fiber morphology (**Appendix A**). We deemed the fiber quality produced was sufficiently promising to proceed with the investigation.

One of the important parameters of centrifugal melt spinning is the melting point of the polymer. Melting point (T_m) of pure 35 000 g/mol PEO was determined to be 66°C, in order to translate this process to PEO-cinnamate, the T_m was determined to be 61°C. With a distinct T_m, PEO-cinnamate fibers were produced using an as-purchased cotton candy machine, which was determined to spin at a fixed rate of ~2300 RPM and were imaged with optical microscopy **(Figure 5.8)**. The average fiber diameter was determined to be 28.9±13.3 μm and the fiber diameters had a normal distribution as shown in **Figure 5.9**.

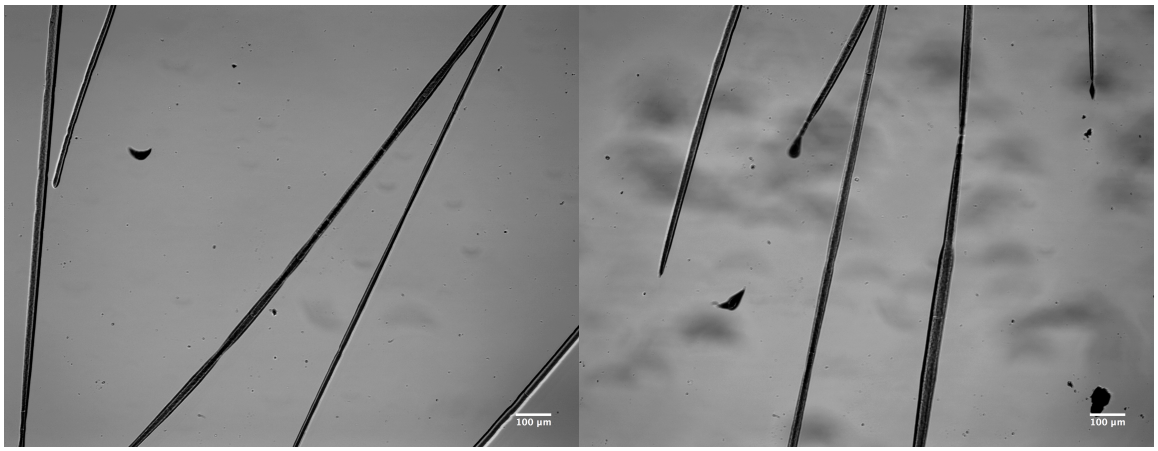

Figure 5.8: Optical microscopy images of PEO-cinnamate fibers produced with the as-purchased cotton candy machine.

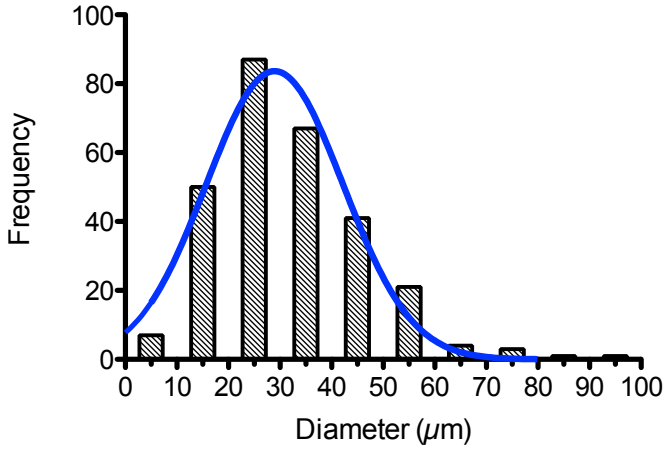

Figure 5.9: Fiber diameter distribution of PEO-cinnamate fibers shown above produced using an as-purchased cotton candy machine.

Although small fiber diameters are critical for tissue engineering applications as it influences cell morphology, migration and stem cell differentiation, the importance of fiber diameter for drug delivery is related to the release rate of drug from the fiber. For diffusion dependent fiber delivery systems, larger diameter fibers may have slower diffusion due to the diffusion distance from the core of the fiber. Also, the surface area to volume ratio is increased for smaller diameter fibers which may enhance drug release [96].

The next fiber production step involved the modification of the spinning set-up. PEO-cinnamate fibers produced using this modified centrifugal melt spinning at 6000 RPM, 45 V for voltage controlled temperature and under ambient conditions with a newly designed spinneret. Images were taken with SEM **(Figure 5.10)**. Fibers produced had a uniform morphology along the fibers and an average fiber diameter was determined to be 11.5±5.5 µm from analysis of 120 fibers of the sample.

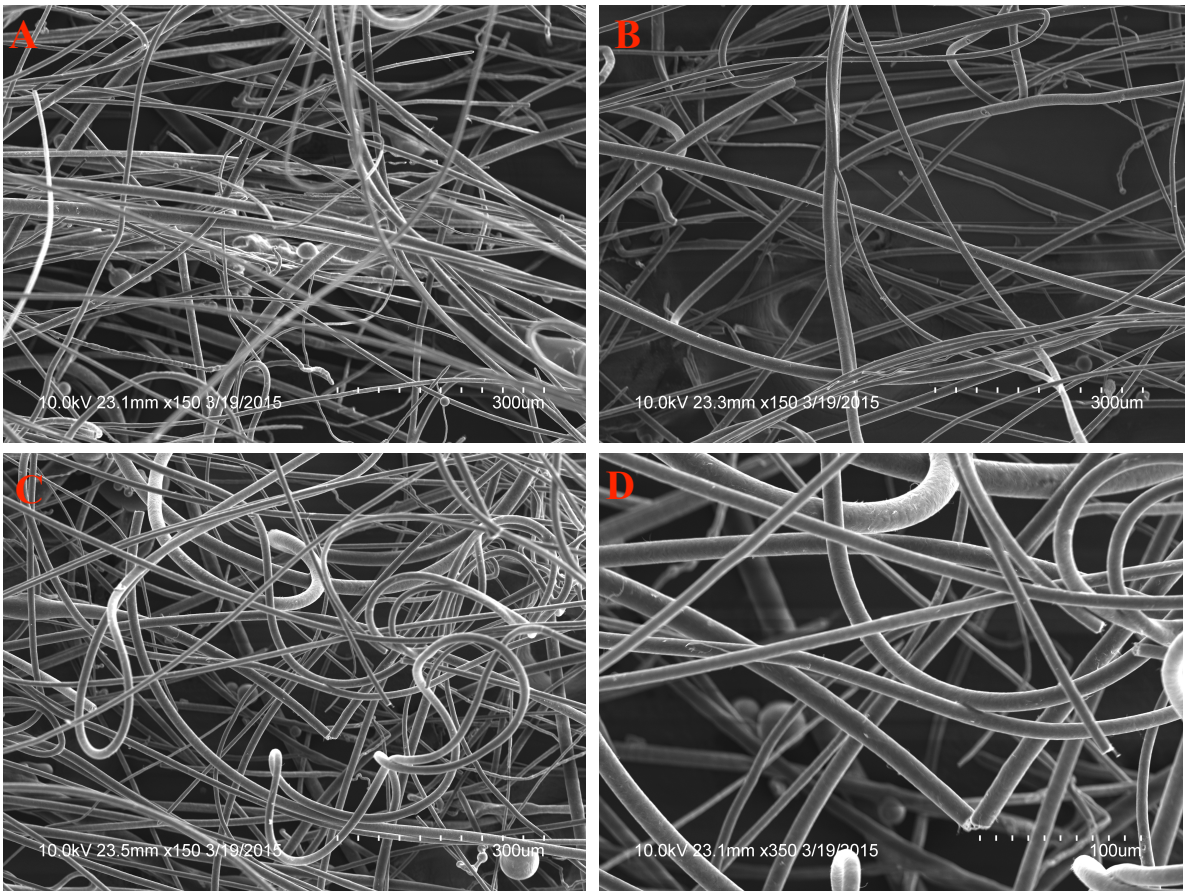

Figure 5.10: Scanning electron microscopy images of PEO-cinnamate fibers produced with modified system and newly designed spinneret at 150X (A-C) and 350X (D) magnifications. Scale bars are 300 µm (A-C) and 100 µm (D).

The fiber diameters were normally distributed as shown in **(Figure 5.11A)**. The values are well described by a Gaussian curve **(Figure 5.11B)**. Therefore, with modifications of the fiber spinning system, the average fiber diameter was reduced and the distribution was narrowed. Although the differences can not be directly

compared given that the imaging modalities differ.

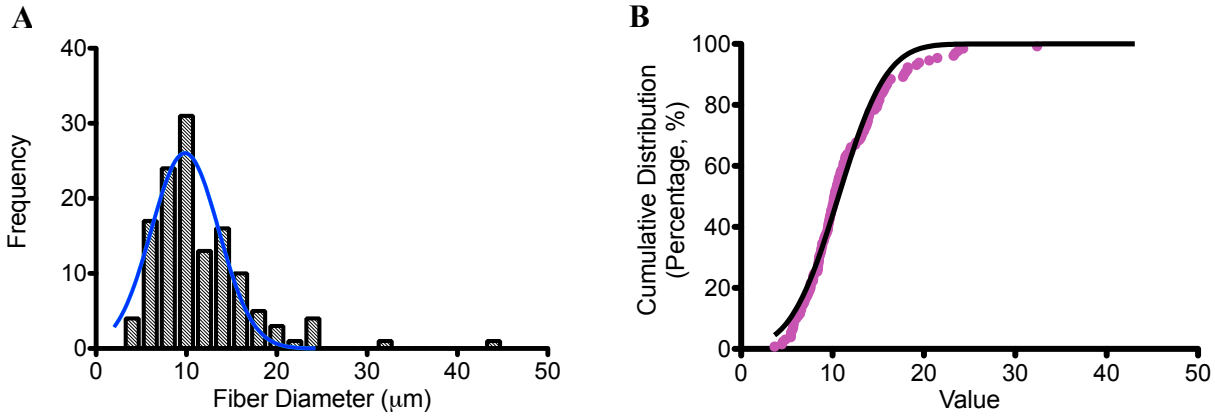

Figure 5.11: Fiber diameter distribution of PEO-cinnamate fibers shown in A, average diameter of 11.5 ± 5.5 μm (n = 130). B presents fiber diameter frequencies (**pink**) in respect to a Gaussian curve (**black**).

These results demonstrate the utility of centrifugal melt spinning for the rapid and facile production of uniform polymeric fibers. Also, the demonstration that fiber diameter was altered through the alteration of the spinneret, indicates the possibility of optimization of the process further to obtain a wide range of diameters by changing that parameter. Additionally, as reported by [48], this fiber production method is controlled by several parameters permitting the future optimization through changes in rotation speed, solution viscosity, environmental temperature and others.

5.3. UV Crosslinking of Fibers

The fibers were irradiated with a 365 nm UV lamp (Cole-Parmer, Canada) at a distance of 5 cm from the source, the shortest distance available with the stand. Using UV/Vis spectroscopy, it was shown that prior to UV exposure, C=C of cinnamate was intact, showing maximum absorbance at 277 nm. Also, PEO which does not possess the C=C shows no absorbance at 277 nm. First, crosslinking was demonstrated on thin films as a proof-of-concept for the time dependency on the degree of crosslinking **(Figure 5.12)**. As the films are exposed to UV for 0, 0.5 and 1 hour, the peak

associated with C=C diminishes, indicating crosslinking. After success with the thin films, we applied this method to the fibers. As the fibers are exposed to 1, 2 and 4 hours of UV, absorbance decreases, indicating breakage of the C=C and non-C=C bond formation suggesting crosslinking had occurred, measurements were made in triplicate and the variability is reflected by the error bars **(Figure 5.13)**. To further demonstrate UV crosslinking of fibers, FTIR spectra of PEO-cinnamate before and after UV irradiation was obtained. A peak at 1640 cm^{-1} corresponding to C=C stretch of cinnamate moieties is reduced **(Figure 5.14)**. Qualitative demonstration of stability, fibers embedded with curcumin were suspended in waters and centrifuged **(Figure 5.17)**. A network is clearly visible as the pellet in the centrifuge tube.

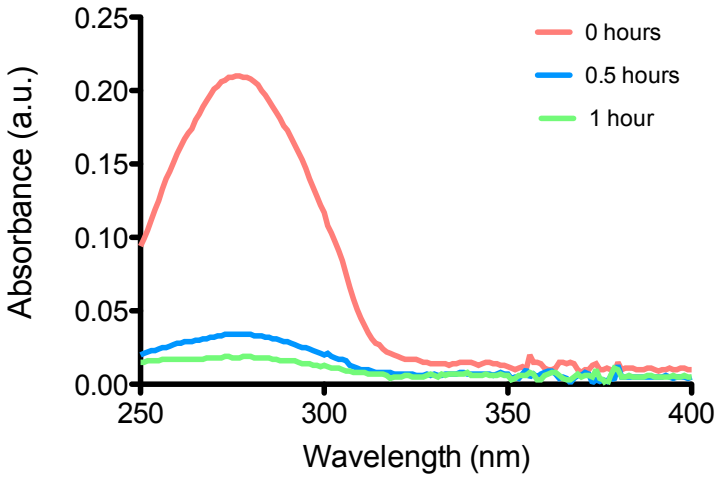

Figure 5.12: UV/Vis spectra of PEO-cinnamate thin films on quartz slides after various lengths (0, 0.5, 1 hour) of UV exposure. The peak at 277 nm is associated with C=C double of cinnamoyl chloride.

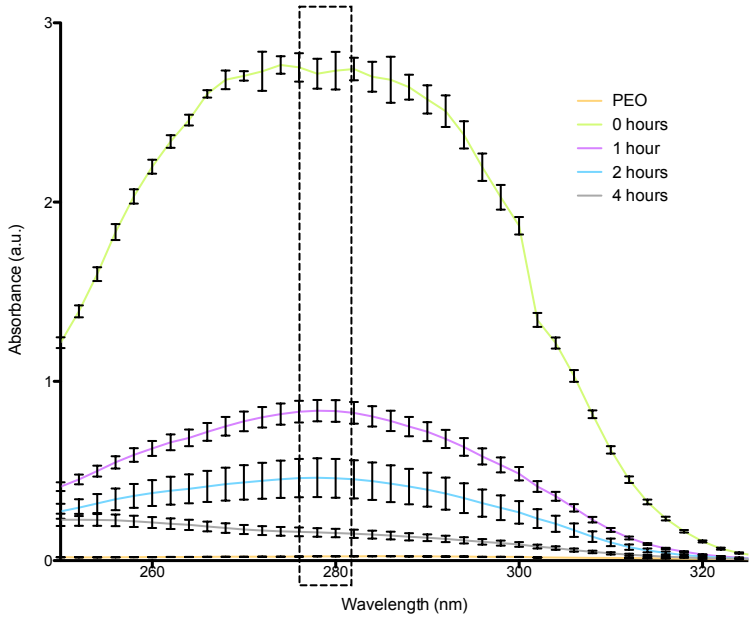

Figure 5.13: UV/Vis spectra of PEO-cinnamate fibers after various lengths (0, 1, 2 and 4 hours) of UV exposure and pure PEO without irradiation. A peak at 277 nm associated with C=C in cinnamate is outlined.

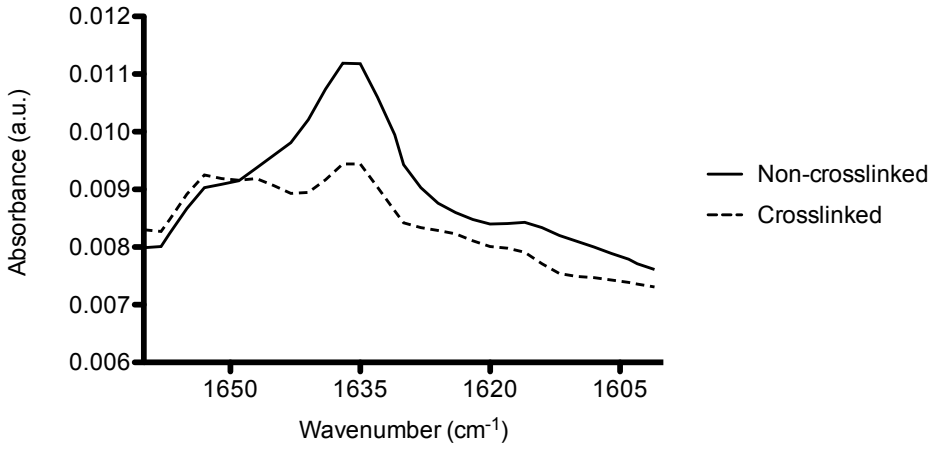

Figure 5.14: FTIR spectrum of PEO-cinnamate before (solid line —) and after 4 hours of UV irradiation (dashed line - -).

Crosslinking is essential for water soluble polymers such as PEO in order to stabilize the polymer for contact to aqueous environments such as any physiological environment. This set of results demonstrates quantitatively and qualitatively the crosslinking of PEO-cinnamate fibers to stabilize them in an aqueous environment. The peaks of UV/Vis spectra at 227 nm look diminished nearly to baseline of PEO, however, there is the possibility of some C=C bonds and uncrosslinked chains remaining. This would be due to steric hindrance, particularly related to the thickness of the film or fibrous mat.

In the future, in order to increase crosslinking efficiency, a UV lamp emitting wavelengths closer 277 nm would be more appropriate. This would decrease the length of time required for crosslinking as the wavelength is closer to the absorption wavelength.

5.4. Curcumin Loading

One of the applications of the stabilized fibers is drug delivery. In order to demonstrate the utility of this material as a drug delivery carrier, investigation of loading and release kinetics was required. First, to determine that loading of curcumin into the fibers effectively occurred after soaking in an ethanolic curcumin solution, the sample was visually observed for a colour change and further analyzed with FTIR to identify the presence of functional groups associated with curcumin not present in the unloaded sample. A sample loaded with curcumin after the excess surface curcumin was washed off is shown in **Figure 5.15**. The bright yellow hue is visually apparent, indicating the presence of curcumin. However, to ensure that the curcumin was not present only on the surface of the swollen fibers, several rinses were performed until the run-off contained no detectable curcumin, suggesting surface curcumin was removed. FTIR analysis revealed a peak at 3425 cm^{-1} corresponding to the phenolic O-H stretch present in curcumin. A peak at 2883 cm^{-1} corresponding to aromatic C-H stretch and is present for both PEO-cinnamate containing and not

containing curcumin. A peak at 1635 cm^{-1} corresponding to the conjugated system for C=O stretch in curcumin was present. A peak at 1466 cm^{-1} corresponding to C-C stretch bond in the ring of aromatic groups of curcumin and PEO-cinnamate were present **(Figure 5.16)**. Thus, it was determined that curcumin was embedded within the fiber.

Figure 5.15: Image of wet bulk fibers loaded with curcumin with a visible yellow hue after washing to remove surface curcumin.

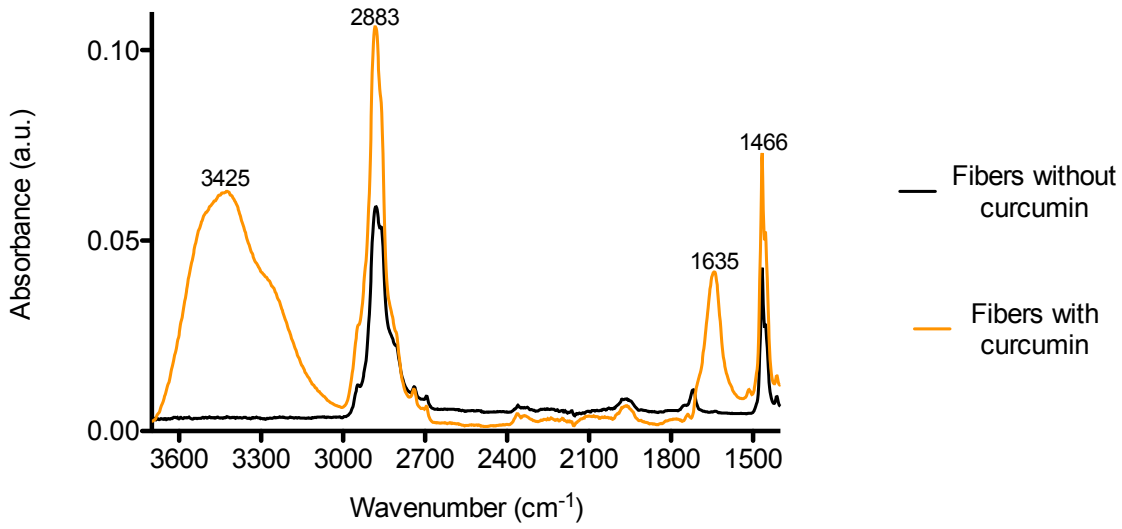

Figure 5.16: FTIR spectrum of crosslinked PEO-cinnamate with (**orange**) and without (**black**) curcumin incorporation.

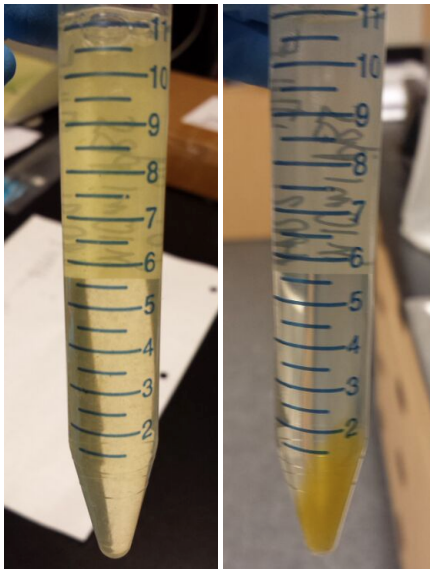

Figure 5.17: Fibers loaded with curcumin in water (**left**) and isolated via centrifugation (**right**) to demonstrate the stability of the fibers in an aqueous environment.

To determine whether the amount of loaded curcumin was tuneable, various concentrations of curcumin in ethanol, 1, 3 and 5 mg/ml were used for loading. It was determined that as loading concentration increased, curcumin loading increased **(Figure 5.18)**. In a loading concentration of 1, 3 and 5 mg/ml, 200 mg of fibers carried 23.89±2.29, 37.32±0.63, 54.32±0.62 μg, respectively. Thus, the amount of curcumin loaded is tuneable based on the curcumin loading concentration and is related to the amount of fibers by mass. To ensure curcumin was maximally drawn out of the fibers, extraction continued until curcumin was undetectable in the supernatant using UV/Vis spectrophotometry measurements at 427 nm, the absorbance wavelength for curcumin [97]. Representative images of the fibers during the first and last wash extractions are shown in **Figure 5.19**.

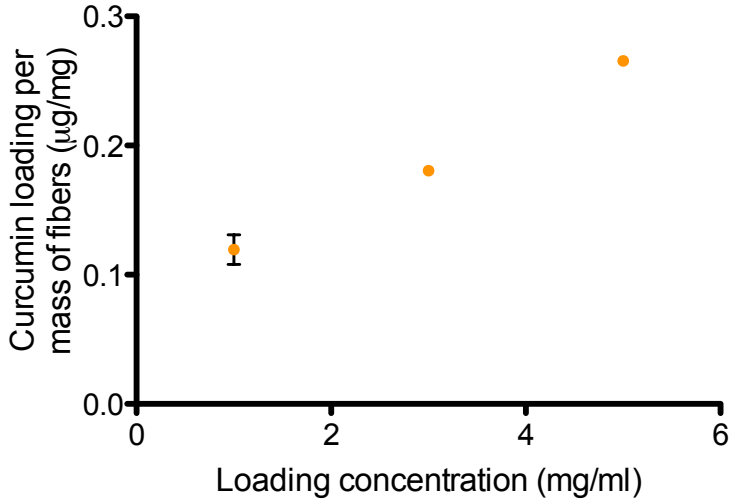

Figure 5.18: Amount of curcumin loaded relative to the concentration of curcumin loading solution.

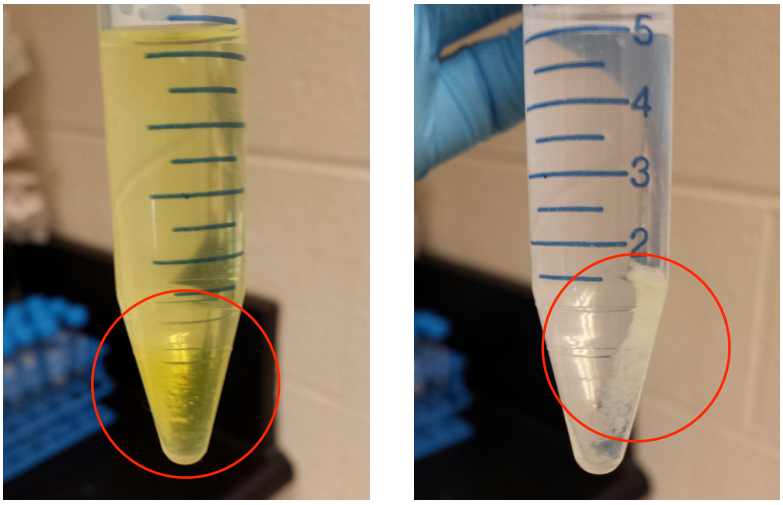

Figure 5.19: Curcumin loaded fibers during the first extraction (**left**) and last extraction (**right**) the red circle identifying the bulk of the fibers.

5.5. *In vitro* Curcumin Releases

Loaded fibers were placed in PBS in a 37°C shaking water bath for 7 and 14 days for fibers loaded in 1 mg/ml and 3 mg/ml solutions, respectively. These end points were selected as consecutive measurements at these time points indicated a plateau, with

no further release. Curcumin release was observed and a release profile was obtained to study the type of release from this polymeric system. It was found that the cumulative amount of curcumin release is dependent on the amount of curcumin loaded as seen with the raw data in **Figure 5.20**. Also, the release profiles do not significantly differ from each other as demonstrated with a two-way ANOVA, comparing the two release curves once scaled based on the final cumulative amount of curcumin extracted (**Figure 5.21**), p = 0.6095, indicating a non-significant difference in the release profiles.

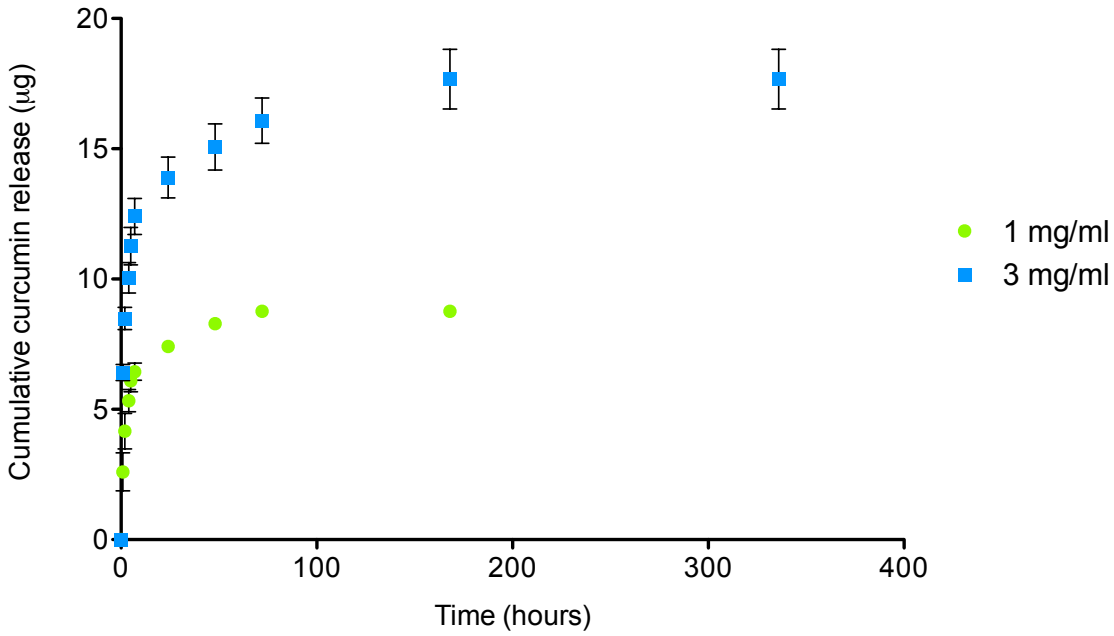

Figure 5.20: Raw data release profiles of PEO-cinnamate fibers loaded in 1 mg/ml (**green**) and 3 mg/ml (**blue**) loading concentrations.

To further characterize the release, using mathematical models to describe the data may be useful. The empirical model described by Ritger and Peppas [98], compares the release profile to a power law. Two fitting parameters k and n are used to fit time, t, to cumulative release from the system, M_t/M_∞. $M_t/M_\infty=kt^n$, where M_t/M_∞ is the amount of drug released, k is the kinetic constant, t is the time for release and n is the diffusional constant. The n-values are of significant importance for relating the

system geometry to the drug release mechanism as shown in **Table 3**. The n-values for both fibers loaded in 1 mg/ml solution and 3 mg/ml solution when fitted to the empirical model, diffusion exponent were 0.48 ± 0.14 and 0.31 ± 0.02, respectively. The fit of this model was reasonable with R^2 values of 0.86 for 1 mg/ml and 0.99 for 3 mg/ml loading.

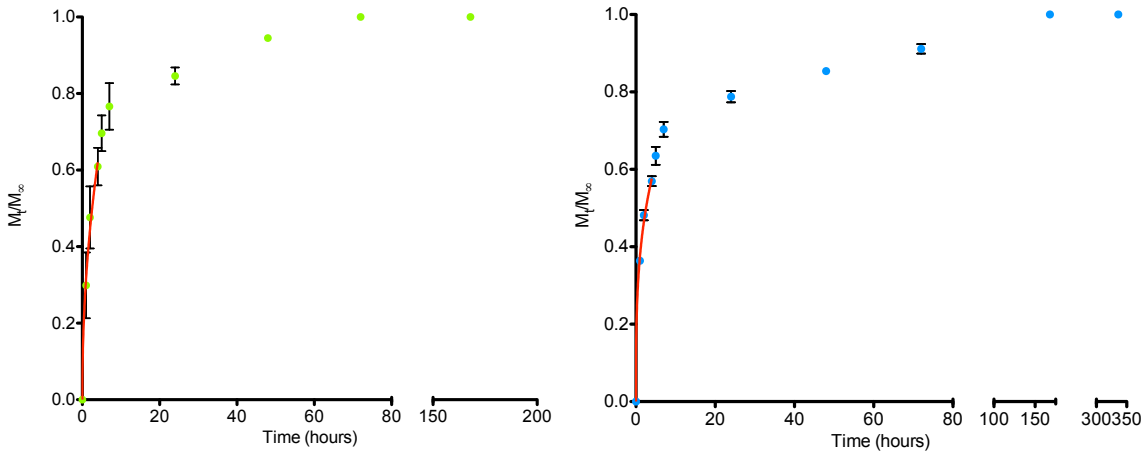

Figure 5.21: Data scaled based on maximum curcumin extracted through release in PBS. Data fitted with Power Law for Mt/Mi ≤ 0.6.

The diffusion coefficient, n, for the 1 mg/ml, according to this model, falls within the range of anomalous (non-Fickian) transport (**Table 3**). For the 3 mg/ml loading, according to this model, does not fall within any of the ranges described. This could be due imperfections in the fiber and thus variable release unpredicted by the model. Further characterization of loaded fiber morphology would be useful. As determined from the two-way ANOVA, these two plots are not significantly different from each other, and thus should exhibit similar non-linear fits. Also, these tests were performed in triplicate, and with further optimization and replicates, the calculated values will become more accurate. Additionally, this data could be fitted to equation 5 of chapter 2. This would allow for the determination of D, the diffusion coefficient which would best describe the diffusivity of curcumin from the system.

Table 3: Diffusion exponent and drug release mechanisms of different geometries

Drug release mechanism	Diffusion Exponent, n		
	Thin film	Cylinder	Sphere
Fickian	0.5	0.45	0.43
Anomalous (non-Fickian) transport	0.5<n<1.0	0.45<n<0.89	0.43<n<0.85
Case-II Transport	1.0	0.89	0.85

5.6. Effect of Free Curcumin on Cells

The A549 cell line was selected based on literature findings and similar intracellular targets to squamous cell carcinomas [99-101]. Although the A549s are not derived from a SCC, the intracellular targets of curcumin are more important and relevant for cell testing. It has been established that drug sensitivity is not tissue-specific when testing cancer cell lines [102].

To determine the dose-dependence of curcumin on cell growth inhibition, an initial range of curcumin concentrations ranging from 0 - 100 uM was selected to treat cells. This starting range was selected based on previous work [99-101]. The initial range of concentrations revealed 100 % effectiveness with concentrations of 15 μM and above (**Figure 5.22**). This value is significantly different from the values previously reported. In the literature, the IC50 value reported is 18 μM [103]. Possible factors contributing to this discrepancy include curcumin purity, and light and heat exposure to samples as curcumin is both light and heat sensitive.

Dose-dependent growth inhibition was observed and the IC10, IC50 and IC90 were determined from these curves (**Figures 5.22 and 5.23**) to be 1.87 ± 0.32 μM , 7.28 ± 0.34 μM, 13.37 ± 0.53 μM, respectively. These values will be useful in determining the amount of curcumin to load into the stabilized PEO-cinnamate fiber drug carrier for preliminary studies. Also, these values may be used as bench marks for comparing the effect of curcumin released from fibers versus free curcumin, as the system may

increase the bioavailability and thus have an increase effect.

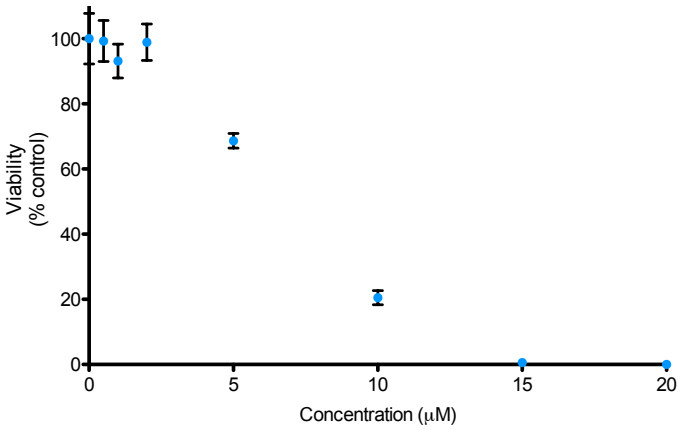

Figure 5.22: Broad range free curcumin dose-response curve.

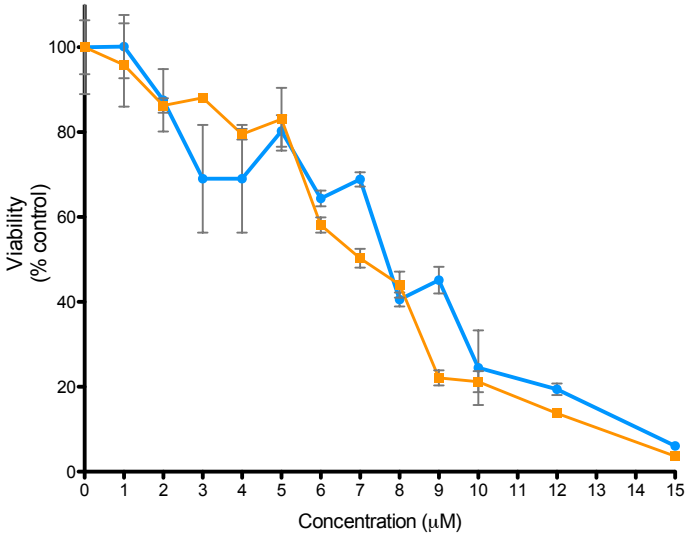

Figure 5.23: Higher resolution free curcumin dose-response curves original batch (**blue**), fresh batch (**orange**).

5.7. Effect of Curcumin Loaded PEO-Cinnamate Fibers

Using the results from the free curcumin dose-dependency study, calculations are prepared as a guideline for moving forward with the study of loaded curcumin on

these cells. Calculations for loading equivalent amounts of curcumin for *in vitro* studies are shown below.

IC 10:

$$= 1.87 \ \frac{\mu mol}{L} \cdot 4 \ ml \cdot 10^{-3} \ \frac{L}{ml} \cdot 10^{-6} \ \frac{mol}{\mu mol} \cdot 368 \ \frac{g}{mol}$$

$$= 2.75 \ \mu g$$

IC 50:

$$= 7.28 \ \frac{\mu mol}{L} \cdot 4 \ ml \cdot 10^{-3} \ \frac{L}{ml} \cdot 10^{-6} \ \frac{mol}{\mu mol} \cdot 368 \ \frac{g}{mol}$$

$$= 10.71 \ \mu g$$

IC 90:

$$= 13.37 \ \frac{\mu mol}{L} \cdot 4 \ ml \cdot 10^{-3} \ \frac{L}{ml} \cdot 10^{-6} \ \frac{mol}{\mu mol} \cdot 368 \ \frac{g}{mol}$$

$$= 19.68 \ \mu g$$

As shown with the range achieved for the loading concentration and actual amount of curcumin loaded into the stabilized fibers (**Figure 5.18**), it is possible for these amounts of curcumin to be incorporated into the stabilized fibers.

6. CONCLUSIONS

We have demonstrated the synthesis of a photosensitive polymer that can undergo UV photocrosslinking for aqueous stability following fiber fabrication using a modified cotton candy machine. Ultimately, this fiber fabrication method presents the potential for a highly scalable method to produce fibers for biomedical purposes, such as drug delivery. The utility of these stabilized fibers for carrying and delivering curcumin has also been demonstrated. And we have demonstrated the relationship between the curcumin loading concentration and amount of curcumin actually loaded. Additionally, the effect of free curcumin in a dose-dependent manner on an A549 cancer cell line has been investigated. Thus, this stabilized polymeric system has the potential to carry a sufficient amount of curcumin for an effective reduction of cancer cell growth.

7. FUTURE DIRECTIONS

There are several future directions and experiments that can follow this work. Some of the major material components to be explored are the swelling and degradation properties of the system. These two parameters effect drug release, are important to define for polymer systems and the characterization of which is essential in fully understanding the system. To further investigate the release of curcumin *in vitro*, in place of PBS, simulated body fluid consisting of proteins would be of interest to determine if the presence of proteins would effect the release of curcumin [104]. These studies could be better predictors of how this system would perform *in vivo*. In addition to studying the release of curcumin *in vitro*, the study of the effect of curcumin is important in establishing a relationship between the drug and cells. One study could be of the antioxidant activity of curcumin, post-release from the polymeric system to ensure the activity remains intact. The 1,1’-diphenyl-2-picrylhydrazyl (DPPH) assay is a possibility and has been shown to be effective in detecting the antioxidant activity of curcumin [96]. The effect of free curcumin on

A549 cells have been established in the work and the concentrations of such an effect has been measured. These values can be used as a guideline for the study of the effect of curcumin loaded into the stabilized fibers on the cells. It would also be of interest to perform these studies on another cell line with similar cellular targets to see if the effects are comparable. And of course, *in vivo* studies with an appropriate animal model would be an important step in evaluating the efficacy of this system after the optimization steps with the *in vitro* studies. These experiments would determine the anti-cancer efficacy of the system and any system related toxicity. One way to study this in a controlled experiment would be to treat areas of nude animal skin with a mutation inducing chemical such as 12-O-tetradecanoylphorbol-13-acetate (TPA) and at various times post-treatment of TPA apply the polymeric system for various lengths of time and evaluate the changes in the skin macroscopically and microscopically with histology.

References

[1] Diepgen TL, Mahler V. The epidemiology of skin cancer. Br J Dermatol 2002;146 Suppl 61:1-6.

[2] Leiter U, Eigentler T, Garbe C. Epidemiology of skin cancer. Adv Exp Med Biol 2014;810:120-40.

[3] Organization WH. How common is skin cancer? Skin cancer 2011.

[4] Phillips JM, Clark C, Herman-Ferdinandez L, Moore-Medlin T, Rong X, Gill JR, et al. Curcumin inhibits skin squamous cell carcinoma tumor growth in vivo. Otolaryngol Head Neck Surg 2011;145:58-63.

[5] Mescher AL. Junqueira's Basic Histology: Text & Atlas, 13e. New York, NY: McGraw-Hill; 2013.

[6] Brash DE. Sunlight and the onset of skin cancer. Trends Genet 1997;13:410-4.

[7] Sturm RA. Skin colour and skin cancer - MC1R, the genetic link. Melanoma Res 2002;12:405-16.

[8] Yoshino M, Nakatsu Y, te Riele H, Hirota S, Kitamura Y, Tanaka K. Additive roles of XPA and MSH2 genes in UVB-induced skin tumorigenesis in mice. DNA Repair (Amst) 2002;1:935-40.

[9] Rowert-Huber J, Patel MJ, Forschner T, Ulrich C, Eberle J, Kerl H, et al. Actinic keratosis is an early in situ squamous cell carcinoma: a proposal for reclassification. Br J Dermatol 2007;156 Suppl 3:8-12.

[10] Ratushny V, Gober MD, Hick R, Ridky TW, Seykora JT. From keratinocyte to cancer: the pathogenesis and modeling of cutaneous squamous cell carcinoma. J Clin Invest 2012;122:464-72.

[11] Trosko JE, Chu EH, Carrier WL. The Induction of Thymine Dimers in Ultraviolet-Irradiated Mammalian Cells. Radiat Res 1965;24:667-72.

[12] Alam M, Ratner D. Cutaneous squamous-cell carcinoma. N Engl J Med 2001;344:975-83.

[13] Lomas A, Leonardi-Bee J, Bath-Hextall F. A systematic review of worldwide incidence of nonmelanoma skin cancer. Br J Dermatol 2012;166:1069-80.

[14] Eisemann N, Waldmann A, Geller AC, Weinstock MA, Volkmer B, Greinert R, et al. Non-melanoma skin cancer incidence and impact of skin cancer screening on incidence. J Invest Dermatol 2014;134:43-50.

[15] Stockfleth E, Peris K, Guillen C, Cerio R, Basset-Seguin N, Foley P, et al. Physician perceptions and experience of current treatment in actinic keratosis. J Eur Acad Dermatol Venereol 2015;29:298-306.

[16] Kelloff GJ, Boone CW, Steele VE, Fay JR, Lubet RA, Crowell JA, et al. Mechanistic considerations in chemopreventive drug development. J Cell Biochem Suppl 1994;20:1-24.

[17] Wright TI, Spencer JM, Flowers FP. Chemoprevention of nonmelanoma skin cancer. J Am Acad Dermatol 2006;54:933-46; quiz 47-50.

[18] Duvoix A, Blasius R, Delhalle S, Schnekenburger M, Morceau F, Henry E, et al. Chemopreventive and therapeutic effects of curcumin. Cancer Lett 2005;223:181-90.

[19] Moon TE, Levine N, Cartmel B, Bangert JL, Rodney S, Dong Q, et al. Effect of retinol in preventing squamous cell skin cancer in moderate-risk subjects: a randomized, double-blind, controlled trial. Southwest Skin Cancer Prevention Study Group. Cancer Epidemiol Biomarkers Prev 1997;6:949-56.

[20] Hansen LA, Sigman CC, Andreola F, Ross SA, Kelloff GJ, De Luca LM. Retinoids in chemoprevention and differentiation therapy. Carcinogenesis 2000;21:1271-9.

[21] Kim DJ, Takasuka N, Nishino H, Tsuda H. Chemoprevention of lung cancer by lycopene. Biofactors 2000;13:95-102.

[22] Katiyar SK. Grape seed proanthocyanidines and skin cancer prevention: inhibition of oxidative stress and protection of immune system. Mol Nutr Food Res 2008;52 Suppl 1:S71-6.

[23] Zhou K, Raffoul JJ. Potential anticancer properties of grape antioxidants. J Oncol 2012;2012:803294.

[24] Kim JW, Amin AR, Shin DM. Chemoprevention of head and neck cancer with green tea polyphenols. Cancer Prev Res (Phila) 2010;3:900-9.

[25] Hu G, Zhang L, Rong Y, Ni X, Sun Y. Downstream carcinogenesis signaling pathways by green tea polyphenols: a translational perspective of chemoprevention and treatment for cancers. Curr Drug Metab 2014;15:14-22.

[26] Singh M, Suman S, Shukla Y. New Enlightenment of Skin Cancer Chemoprevention through Phytochemicals: In Vitro and In Vivo Studies and the Underlying Mechanisms. Biomed Res Int 2014;2014:243452.

[27] Terlikowska K, Witkowska A, Terlikowski S. [Curcumin in chemoprevention of breast cancer]. Postepy Hig Med Dosw (Online) 2014;68:571-8.

[28] Ammon HP, Wahl MA. Pharmacology of Curcuma longa. Planta Med 1991;57:1-7.

[29] Srinivasan KR. The colouring matter in turmeric. Current Science 1952;311.

[30] Kiuchi F, Goto Y, Sugimoto N, Akao N, Kondo K, Tsuda Y. Nematocidal activity of turmeric: synergistic action of curcuminoids. Chem Pharm Bull (Tokyo) 1993;41:1640-3.

[31] Tayyem RF, Heath DD, Al-Delaimy WK, Rock CL. Curcumin content of turmeric and curry powders. Nutr Cancer 2006;55:126-31.

[32] Kunnumakkara AB, Anand P, Aggarwal BB. Curcumin inhibits proliferation, invasion, angiogenesis and metastasis of different cancers through interaction with multiple cell signaling proteins. Cancer Lett 2008;269:199-225.

[33] Cheng AL, Hsu CH, Lin JK, Hsu MM, Ho YF, Shen TS, et al. Phase I clinical trial of curcumin, a chemopreventive agent, in patients with high-risk or pre-malignant lesions. Anticancer Res 2001;21:2895-900.

[34] Garcea G, Jones DJ, Singh R, Dennison AR, Farmer PB, Sharma RA, et al. Detection of curcumin and its metabolites in hepatic tissue and portal blood of patients following oral administration. Br J Cancer 2004;90:1011-5.

[35] Sharma RA, McLelland HR, Hill KA, Ireson CR, Euden SA, Manson MM, et al. Pharmacodynamic and pharmacokinetic study of oral Curcuma extract in patients with colorectal cancer. Clin Cancer Res 2001;7:1894-900.

[36] Jiao Y, Wilkinson Jt, Christine Pietsch E, Buss JL, Wang W, Planalp R, et al. Iron chelation in the biological activity of curcumin. Free Radic Biol Med 2006;40:1152-60.

[37] Jiao Y, Wilkinson Jt, Di X, Wang W, Hatcher H, Kock ND, et al. Curcumin, a cancer chemopreventive and chemotherapeutic agent, is a biologically active iron chelator. Blood 2009;113:462-9.

[38] Caro JJ, Salas M, Ward A, Goss G. Anemia as an independent prognostic factor for survival in patients with cancer: a systemic, quantitative review. Cancer 2001;91:2214-21.

[39] Huang MT, Lysz T, Ferraro T, Abidi TF, Laskin JD, Conney AH. Inhibitory effects of curcumin on in vitro lipoxygenase and cyclooxygenase activities in mouse epidermis. Cancer Res 1991;51:813-9.

[40] Kuttan R, Sudheeran PC, Josph CD. Turmeric and curcumin as topical agents in cancer therapy. Tumori 1987;73:29-31.

[41] Sonavane K, Phillips J, Ekshyyan O, Moore-Medlin T, Roberts Gill J, Rong X, et al. Topical curcumin-based cream is equivalent to dietary curcumin in a skin cancer model. J Skin Cancer 2012;2012:147863.

[42] Sugerman DT. JAMA patient page. Chemotherapy. JAMA 2013;310:218.

[43] Heller J, Hoffman AS. Biomaterials Science: An introduction to materials in medicine. 2 ed. London, UK: Elsevier Academic Press; 2004.

[44] Baker RW, and Lonsdale, H.K. Controlled release: mechanisms and rates. Controlled release of biologically active agents 1974:15-71.

[45] Kunwar A, Barik A, Mishra B, Rathinasamy K, Pandey R, Priyadarsini KI. Quantitative cellular uptake, localization and cytotoxicity of curcumin in normal and tumor cells. Biochim Biophys Acta 2008;1780:673-9.

[46] Shishodia S, Amin HM, Lai R, Aggarwal BB. Curcumin (diferuloylmethane) inhibits constitutive NF-kappaB activation, induces G1/S arrest, suppresses proliferation, and induces apoptosis in mantle cell lymphoma. Biochem Pharmacol 2005;70:700-13.

[47] Syng-Ai C, Kumari AL, Khar A. Effect of curcumin on normal and tumor cells: role of glutathione and bcl-2. Mol Cancer Ther 2004;3:1101-8.

[48] Luo CJ, Stoyanov SD, Stride E, Pelan E, Edirisinghe M. Electrospinning versus fibre production methods: from specifics to technological convergence. Chem Soc Rev 2012;41:4708-35.

[49] Zeugolis DI, Paul RG, Attenburrow G. Extruded collagen-polyethylene glycol fibers for tissue engineering applications. J Biomed Mater Res B Appl Biomater 2008;85:343-52.

[50] Perale G, Pertici G, Giordano C, Daniele F, Masi M, Maccagnan S. Nondegradative microextrusion of resorbable polyesters for pharmaceutical

and biomedical applications: The cases of poly−lactic−acid and poly−caprolactone. Journal of applied polymer science 2008;108:1591-5.

[51] Yoshimoto H, Shin YM, Terai H, Vacanti JP. A biodegradable nanofiber scaffold by electrospinning and its potential for bone tissue engineering. Biomaterials 2003;24:2077-82.

[52] Yang F, Murugan R, Wang S, Ramakrishna S. Electrospinning of nano/micro scale poly(L-lactic acid) aligned fibers and their potential in neural tissue engineering. Biomaterials 2005;26:2603-10.

[53] Boland ED, Matthews JA, Pawlowski KJ, Simpson DG, Wnek GE, Bowlin GL. Electrospinning collagen and elastin: preliminary vascular tissue engineering. Front Biosci 2004;9:1422-32.

[54] Huang C, Soenen SJ, van Gulck E, Vanham G, Rejman J, Van Calenbergh S, et al. Electrospun cellulose acetate phthalate fibers for semen induced anti-HIV vaginal drug delivery. Biomaterials 2012;33:962-9.

[55] Unnithan AR, Barakat NA, Pichiah PB, Gnanasekaran G, Nirmala R, Cha YS, et al. Wound-dressing materials with antibacterial activity from electrospun polyurethane-dextran nanofiber mats containing ciprofloxacin HCl. Carbohydr Polym 2012;90:1786-93.

[56] Li M, Mondrinos MJ, Chen X, Lelkes PI. Electrospun blends of natural and synthetic polymers as scaffolds for tissue engineering. Conf Proc IEEE Eng Med Biol Soc 2005;6:5858-61.

[57] Guo G, Fu S, Zhou L, Liang H, Fan M, Luo F, et al. Preparation of curcumin loaded poly(epsilon-caprolactone)-poly(ethylene glycol)-poly(epsilon-caprolactone) nanofibers and their in vitro antitumor activity against Glioma 9L cells. Nanoscale 2011;3:3825-32.

[58] Cardoso GB, Machado-Silva AB, Sabino M, Santos AR, Jr., Zavaglia CA. Novel hybrid membrane of chitosan/poly (epsilon-caprolactone) for tissue engineering. Biomatter 2014;4.

[59] Christen AG, Christen JA. William J. Morrison (1860-1926): co-inventor of the cotton candy machine. J Hist Dent 2005;53:51-6.

[60] Badrossamay MR, McIlwee HA, Goss JA, Parker KK. Nanofiber assembly by rotary jet-spinning. Nano Lett 2010;10:2257-61.

[61] Badrossamay MR, Balachandran K, Capulli AK, Golecki HM, Agarwal A, Goss JA, et al. Engineering hybrid polymer-protein super-aligned nanofibers via rotary jet spinning. Biomaterials 2014;35:3188-97.

[62] X. Z, Lu Y. Centrifugal Spinning: An Alternative Approach to Fabricate Nanofibers at High Speed and Low Cost. Polymer Reviews 2014;54:677-701.

[63] Huttunen M, Kellomaki M. A simple and high production rate manufacturing method for submicron polymer fibres. J Tissue Eng Regen Med 2011;5:e239-43.

[64] Moutos FT, Freed LE, Guilak F. A biomimetic three-dimensional woven composite scaffold for functional tissue engineering of cartilage. Nat Mater 2007;6:162-7.

[65] Asher DM. The transmissible spongiform encephalopathy agents: concerns and responses of United States regulatory agencies in maintaining the safety of biologics. Dev Biol Stand 1999;100:103-18.

[66] Meade KR, Silver FH. Immunogenicity of collagenous implants. Biomaterials 1990;11:176-80.

[67] Yang C, Hillas PJ, Baez JA, Nokelainen M, Balan J, Tang J, et al. The application of recombinant human collagen in tissue engineering. BioDrugs 2004;18:103-19.

[68] Hatakeyama H, Tatsuko H. Interaction between water and hydrophilic polymers. Thermochimica acta 1998;308:3-22.

[69] Oh SH, Kang SG, Kim ES, Cho SH, Lee JH. Fabrication and characterization of hydrophilic poly(lactic-co-glycolic acid)/poly(vinyl alcohol) blend cell scaffolds by melt-molding particulate-leaching method. Biomaterials 2003;24:4011-21.

[70] Shen LQ, al. e. Ultrafiltration hollow fiber membranes of sulfonated polyetherimide/polyetherimide blends: preparation, morphologies and anti-fouling properties. Journal of Membrane Science 2003;218:279-93.

[71] Spitzer M, Edvaldo S, Loh W. Poly (ethylene glycol) or Poly (ethylene oxide)?: Magnitude of end-group Contribution to the Partitioning of Ethylene Oxide Oligomers and Polymers between Water and Organic Phases. Journal of the Brazilian Chemical Society 2002;13:7-9.

[72] Sofia SJ, Premnath VV, Merrill EW. Poly(ethylene oxide) Grafted to Silicon Surfaces: Grafting Density and Protein Adsorption. Macromolecules 1998;31:5059-70.

[73] Zheltonozhskaya T, et al. Micellar nanocontainers based on PAAm-b-PEO-b-PAAm triblock copolymers for poorly soluble drugs. European Polymer Journal 2013;49:405-18.

[74] Torchilin VP, et al. Poly(ethylene glycol) on the liposome surface: on the mechanism of polymer-coated liposome longevity. Biochimica et biophysica acta 1994;1995:11-20.

[75] Knop K, Hoogenboom R, Fischer D, Schubert US. Poly(ethylene glycol) in drug delivery: pros and cons as well as potential alternatives. Angew Chem Int Ed Engl 2010;49:6288-308.

[76] Lee JH, Kopecek J, Andrade JD. Protein-resistant surfaces prepared by PEO-containing block copolymer surfactants. J Biomed Mater Res 1989;23:351-68.

[77] Lapienis G. Star-shaped polymers having PEO arms. Progress in Polymer Science 2009;34:852-92.

[78] Liu X, Jin X, Ma PX. Nanofibrous hollow microspheres self-assembled from star-shaped polymers as injectable cell carriers for knee repair. Nat Mater 2011;10:398-406.

[79] Roovers J. Concentration dependence of the relative viscosity of star polymers. Macromolecules 1994;27:5359-64.

[80] She W, et al. PEGylated dendrimer–doxorubicin conjugates as pH-sensitive drug delivery systems: synthesis and in vitro characterization. Journal of Biomedical Nanotechnology 2015;11:964-78.

[81] Fuertges F, and Abraham Abuchowski. The clinical efficacy of poly (ethylene glycol)-modified proteins. Journal of controlled release 1990;11:139-48.

[82] Seth P, Stamm A. Solid compositions containing polyethylene oxide and an active ingredient. Google Patents; 2000.

[83] Fessel G, Cadby J, Wunderli S, van Weeren R, Snedeker JG. Dose- and time-dependent effects of genipin crosslinking on cell viability and tissue mechanics - toward clinical application for tendon repair. Acta Biomater 2014;10:1897-906.

[84] Harris R, Lecumberri E, Heras A. Chitosan-genipin microspheres for the controlled release of drugs: clarithromycin, tramadol and heparin. Mar Drugs 2010;8:1750-62.

[85] Hoare TR, Kohane DS. Hydrogels in drug delivery: Progress and challenges. Polymer 2008;49:1993-2007.

[86] Sung S-J, et al. Two different reaction mechanisms of cinnamate side groups attached to the various polymer backbones. Polymer 2006;47:2314-21.

[87] Ko JH, et al. Characterization of cross-linked gelatin nanofibers through electrospinning. Macromolecular research 2010;18:137-43.

[88] Gupta Pea. In situ photo-cross-linking of cinnamate functionalized poly (methyl methacrylate-co-2-hydroxyethyl acrylate) fibers during electrospinning. Macromolecules 2004;37:9211-8.

[89] Hoskins JA. The occurrence, metabolism and toxicity of cinnamic acid and related compounds. J Appl Toxicol 1984;4:283-92.

[90] Nutley BP, Farmer P, Caldwell J. Metabolism of trans-cinnamic acid in the rat and the mouse and its variation with dose. Food Chem Toxicol 1994;32:877-86.

[91] Nakayama YaM, Takehisa. Preparation and characterization of photocrosslinkable hydrophilic polymer having cinnamate moiety. Journal of polymer science part A: polymer chemistry 1992;30:2451-357.

[92] Holliday DL, Speirs V. Choosing the right cell line for breast cancer research. Breast Cancer Res 2011;13:215.

[93] Godin B, Touitou E. Transdermal skin delivery: predictions for humans from in vivo, ex vivo and animal models. Adv Drug Deliv Rev 2007;59:1152-61.

[94] Phillips J, Moore-Medlin T, Sonavane K, Ekshyyan O, McLarty J, Nathan CA. Curcumin inhibits UV radiation-induced skin cancer in SKH-1 mice. Otolaryngol Head Neck Surg 2013;148:797-803.

[95] Hoskins JA, Holliday SB, Greenway AM. The metabolism of cinnamic acid by healthy and phenylketonuric adults: a kinetic study. Biomed Mass Spectrom 1984;11:296-300.

[96] Suwantong O, Ruktanonchai U, Supaphol P. In vitro biological evaluation of electrospun cellulose acetate fiber mats containing asiaticoside or curcumin. J Biomed Mater Res A 2010;94:1216-25.

[97] Priyadarsini KI. The chemistry of curcumin: from extraction to therapeutic agent. Molecules 2014;19:20091-112.

[98] Ritger PL, Peppas NA. A simple equation for description of solute release II. Fickian and anomalous release from swellable devices. Journal of controlled release 1987;5:37-42.

[99] Lee J, Im YH, Jung HH, Kim JH, Park JO, Kim K, et al. Curcumin inhibits interferon-alpha induced NF-kappaB and COX-2 in human A549 non-small cell lung cancer cells. Biochem Biophys Res Commun 2005;334:313-8.

[100] Lin SS, Lai KC, Hsu SC, Yang JS, Kuo CL, Lin JP, et al. Curcumin inhibits the migration and invasion of human A549 lung cancer cells through the inhibition of matrix metalloproteinase-2 and -9 and Vascular Endothelial Growth Factor (VEGF). Cancer Lett 2009;285:127-33.

[101] Chen Q, Wang Y, Xu K, Lu G, Ying Z, Wu L, et al. Curcumin induces apoptosis in human lung adenocarcinoma A549 cells through a reactive oxygen species-dependent mitochondrial signaling pathway. Oncol Rep 2010;23:397-403.

[102] Jaeger S, Duran-Frigola M, Aloy P. Drug sensitivity in cancer cell lines is not tissue-specific. Molecular Cancer 2015;14:1-4.

[103] Zhang J, Qi H, Wu C. [Research of anti-proliferation of curcumin on A549 human lung cancer cells and its mechanism]. Zhong Yao Cai 2004;27:923-7.

[104] Marques MRC, Loebenberg R, Almukainzi M. Simulated biological fluids with possible application in dissolution testing. Dissolution Technology 2011;18:15-28.

APPENDICES

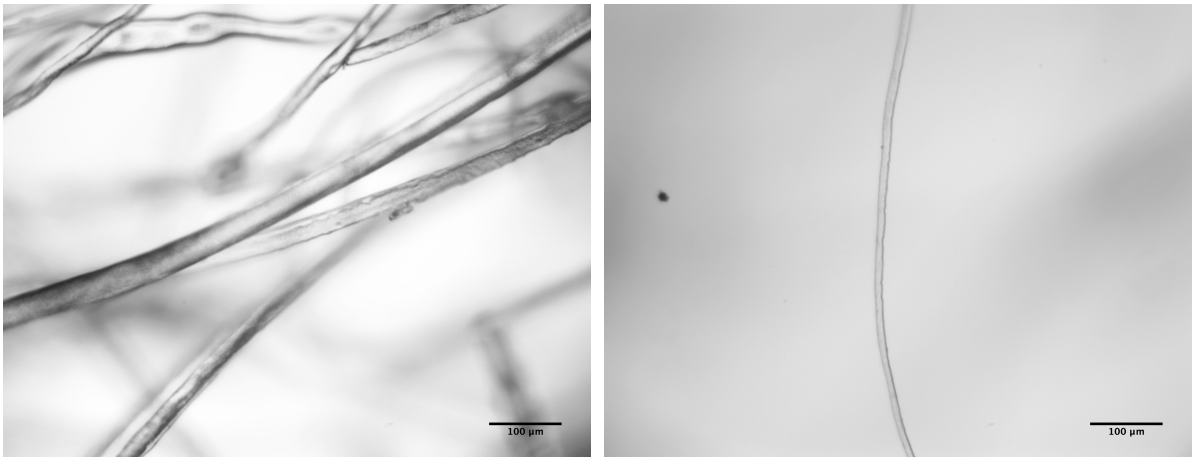

Appendix A: As-spun PEO fibers fabricated using a modified cotton candy machine. Scale bar for the right image is 50 µm.

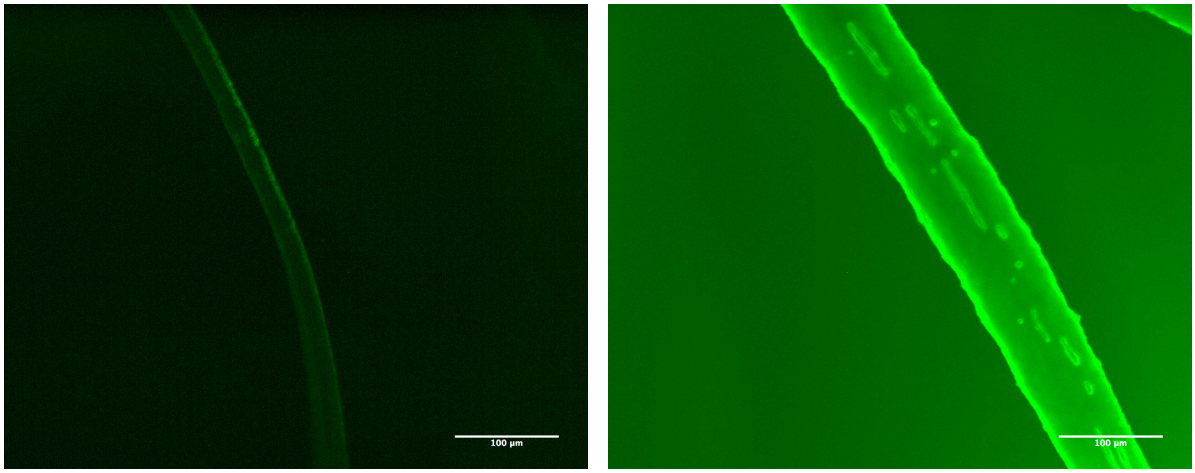

Appendix B: Fluorescence images of stabilized PEO-cinnamate fibers dry and in water. Although the certainty of whether these two fibers are identical, there is a visible size difference. Scale bars for both images at 100 µm.

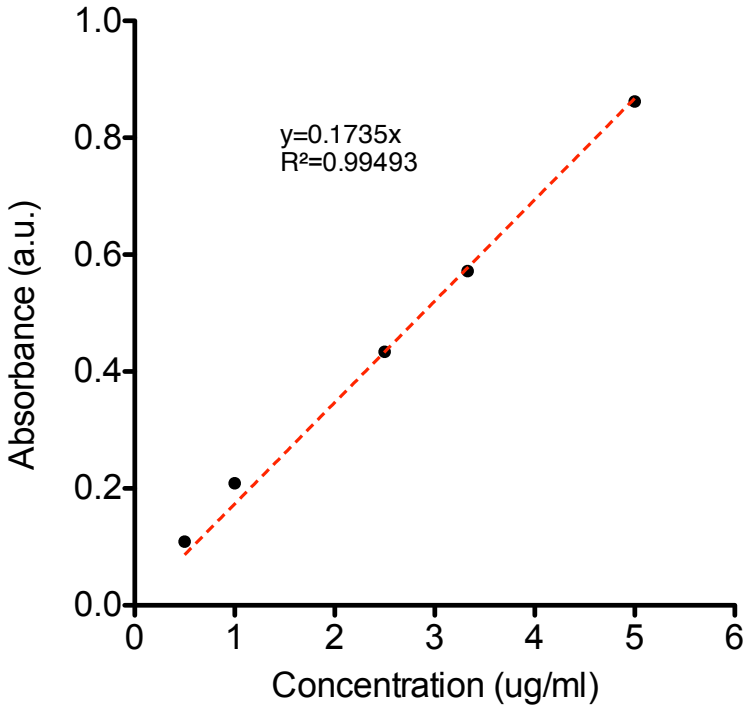

Appendix C: UV/Vis calibration curve for curcumin in ethanol.

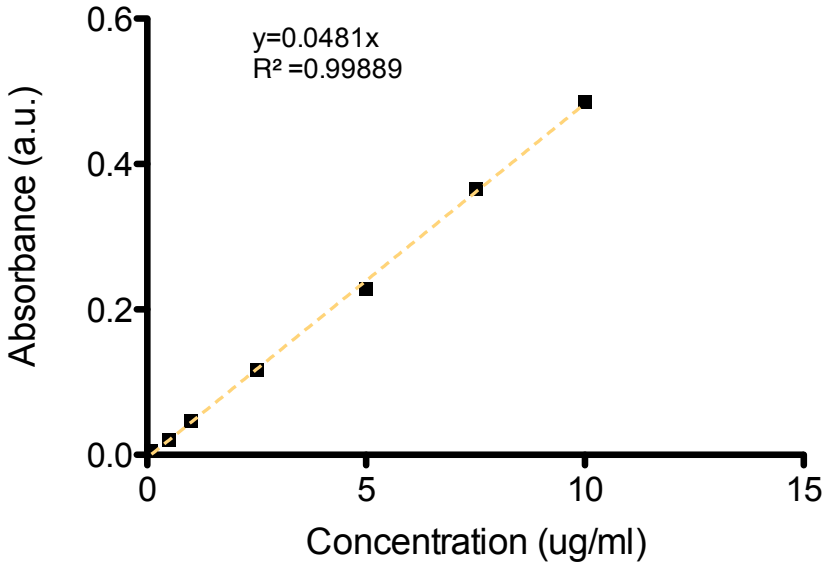

Appendix D: UV/Vis calibration curve for curcumin in phosphate buffered saline.

Curriculum Vitae

Name: Julie La

Post-secondary Education and Degrees:

The University of Western Ontario
London, Ontario, Canada
2013-2015 M.E.Sc.
Thesis:

The University of Western Ontario
London, Ontario, Canada
2009-2013 B.M.Sc.
Honours thesis: *Placental inflammatory response to intermittent umbilical cord occlusions in preterm fetal sheep*

Honours and Awards:

Western Graduate Research Scholarship
University of Western Ontario, 2013-present

Dean's Honour List
University of Western Ontario, 2010-2013

Science Students' Council Impact Award of Merit
University of Western Ontario, 2012

University of Ontario Bursaries - Sciences
University of Western Ontario, 2011, 2012

Ontario Die Company Scholarship
University of Western Ontario, 2009, 2011

Queen Elizabeth II Aiming for the Top Scholarship
University of Western Ontario, 2009

W.C. Rehkopf Memorial Scholarship
University of Western Ontario, 2009

Oral and Poster Presentations:

J. La*, S. Karamdoust, H. Mak, W. Wan, "Drug delivery of curcumin via microfibers for the treatment of skin cancer". Oral Presentation. Canadian Biomaterials Society Annual Meeting. Toronto, Ontario. 29 May 2015.

J. La*, S. Karamdoust, H. Mak, W. Wan, "Fiber production and UV crosslinking of cinnamoyl chloride functionalized poly(ethylene oxide) using centrifugal melt spinning for biomedical applications". Oral Presentation. Biomedical Engineering Department Seminar, London, Ontario, February 2015.

J. La*, S. Karamdoust, H. Mak, W. Wan, "Poly(ethylene oxide) microfiber production via centrifugal spinning and UV stabilization". Poster Presentation. Western Interdisciplinary Research Showcase, London, Ontario. 2 December 2014

A. Golin*, J. Liu, J. La*, W. Wan. "Effect of humidity on electrospun core-shell nanofibers for tissue engineering". Poster Presentation. Canadian Biomaterials Society Meeting Halifax, Nova Scotia. 6 June 2014.

J. La*. “Introduction to Biomedical Engineering”. Oral Presentation. ES1050 Engineering Design Lecture - Graduate Student Series. London, Ontario. March 2014

J. La*, W. Wan, “Cytocompatibility of aligned electrospun collagen nanofibers embedded with growth factors for tympanic membrane regeneration”. Seminar Presentation. Biomedical Engineering Department Seminar, London, Ontario. March 2014.

Related Work Experience:

Graduate Teaching Assistant
The University of Western Ontario
Introductory Design and Innovation Studio 1050
Department of Electrical Engineering
2013, 2014

Graduate Teaching Assistant
The University of Western Ontario
Biophysics of Transport Systems 3501/9501
Department of Medical Biophysics
2014

Research Assistant to Drs. Gurinder Sangha and Roger Zemek
London Health Sciences Centre
Prognosticators of persistent concussion symptoms following pediatric minor traumatic head injury
2013-2015

Research Assistant to Dr. Bryan Richardson
The University of Western Ontario
The effect of maternal nutrition of fetal guinea pig development
Department of Physiology
Children’s Health Research Institute
2012, 2013

Research Assistant to Dr. Edmund Lui
The University of Western Ontario
Immunostimulatory and immunosuppressive effects of ginseng
Department of Physiology and Pharmacology
Ontario Ginseng Innovative Research Consortium

Professional Memberships:

Canadian Biomaterials Society
Student member
2014 - present